THE

METAL-ELECTROLYTE

INTERFACE

by

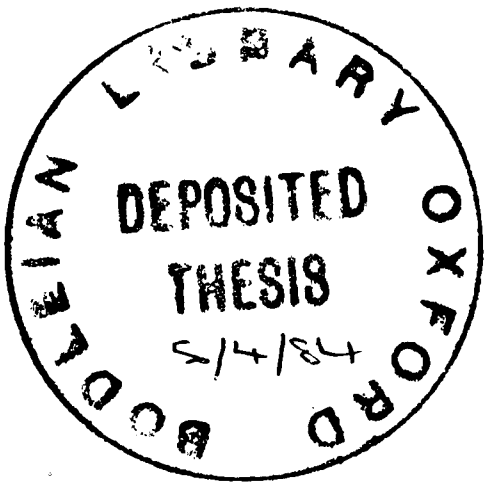
Katharine Painter

Linacre College

Oxford

A thesis submitted for the degree of

Doctor of Philosophy at Oxford University



Michaelmas Term

1983

Theoretical Chemistry

Department

Abstract

THE METAL-ELECTROLYTE INTERFACE

Katharine Painter, Linacre College
D. Phil.
Michaelmas Term, 1983

Theories of the metal-electrolyte interface are reviewed with particular attention to the prediction of thermodynamic quantities. A comparison of the different theories is made using a range of experimental results on Hg-aqueous electrolyte systems. Certain widespread failings of the models are revealed. These are identified as being the results of a neglect of solvent structure and of chemical interactions.

Next a solvent-free metal-molten salt system is investigated using a model based on the MSA. Thermodynamic properties, particularly the capacitance and the potential at the point of zero charge and their variation with temperature, are calculated. The magnitudes for a range of ionic species are in agreement with experiments for Pb-alkali halide systems, but the (relatively weak) temperature dependence is not predicted correctly. The success of this application of the MSA compared to applications to aqueous systems shows the great importance of the solvent in determining the properties of these systems.

To attempt to improve on the MSA model a new model based on the EXP approximation is developed. The predicted trend of the temperature dependence of capacitance is now given correctly but in other respects the predictions are worse than those of the MSA.

In our first MSA model the metal is treated as a hard wall. A more realistic representation is now introduced which incorporates electron spill-out. By a phenomenological analysis the extent of spill-out into the electrolyte is estimated. No direct measurement of this quantity has been made. It is consistent with theoretical estimates made for aqueous systems when allowance is made for the effect of the solvent.

Acknowledgements

I would like to thank my supervisor, Professor N. H. March, who, together with Professor M. P. Tosi, proposed this research project and gave me supervision and encouragement throughout. In addition, I am grateful to them for making available to me the manuscript of their forthcoming book 'Charged Liquids'.

Special thanks are due to Drs. P. J. Grout, S. J. Hemingway and G. Senatore for many useful discussions and helpful comments on the manuscript of this thesis. Acknowledgements must also go to Pietro Ballone and Georgio Pastore for their assistance with the calculations presented in Chapter 4.

I am grateful to the S.E.R.C. for a research studentship and to S.I.S.S.A. for financing my visit to Trieste during which much of the computational work was carried out.

CONTENTS

		Page
Chapter 1:	Introduction	1
1.1	The ideally polarised interface	2
Chapter 2:	Theories of the hard wall-aqueous elect-rolyte interface	8
2.1	Gouy-Chapman theory and its extensions . .	9
2.2	Application of approximate integral equations to the interface region	16
Chapter 3:	Comparison of theoretical and experimental results for metal-aqueous electrolyte interfaces	26
3.1	The experimental system	27
3.2	Comparison of predicted and experimental capacitances	29
3.2.1	The magnitude of the capacitance	29
3.2.2	The concentration and temperature dependence of the capacitance	32
3.3	The compact layer	35
Chapter 4:	The mean spherical approximation for molten alkali halides near a hard wall	43
4.1	Preliminary considerations	44
4.2	The Ornstein-Zernike equation for a two-component system in contact with a hard wall	49
4.3	The MSA for a mixture of ions in contact with a hard wall	52
4.4	Numerical results for the MSA	57
4.5	Beyond the MSA	64
Chapter 5:	The role of the metal	68
5.1	The jellium model for the free metal surface	69
5.2	Electron spill-out at the metal-electrolyte interface	76

5.3 Phenomenological treatment of the electron spill-out 83

Chapter 6: Future work 89

Appendices to Chapter 4

Appendix A: The Baxter technique 93

Appendix B: Analytic result for the capacitance in the MSA 96

Appendix C: Separation of the MSA capacitance into compact and diffuse layer contributions 99

Appendix D: The exponential approximation applied to a two-component system near a hard wall 100

References 105

Chapter 1 Introduction

Electrochemistry is a broad-ranging subject which may be divided into two parts, electrodics and ionics[1]. Electrodics is the study of the interfacial region between an electrode and an electrolyte and, at present, progress in most fields of electrochemistry is determined by our understanding of this subject. Although the study of bulk electrolytes - ionics - is far from complete, because it involves only homogeneous systems it is much further advanced than the study of electrodics. Thus, most current research effort, including the present work, is directed at improving our understanding of the complex subject of electrodics. This field is intrinsically interesting and in addition is of technological importance since the chemical reactions which occur at electrodes are a potentially important source of electrical energy. Many technological applications have now been made[2]. Of particular interest are fuel cells which can directly convert the chemical energy of hydrocarbon fuels to electricity. Electricity was first obtained electrochemically from hydrogen and oxygen by Grove in 1839[3], but it was only recently, when the efficiency of the conversion was increased dramatically, that the usefulness of this method was fully realised. Outside the energy field, electrodics is commercially important for the electroplating of metals, for the production of several industrial chemicals and for the extraction of many reactive metals from their ores. It is also of interest because corrosion is usually an electrochemical process[4].

A considerable amount of work has been done throughout the present century on metal-electrolyte interfaces and the reactions

which occur at them. However, we are still far from a complete understanding at a molecular level. In this work we will be looking particularly at the structure of the interface since it affects the electrodic reactions, although we will not be concerned with the chemistry of the reactions themselves. In the remainder of this chapter we shall attempt to provide a precise definition of the class of interfaces whose structure will later be investigated; some of the thermodynamic relations for these interfaces will also be presented.

1.1 The ideally polarised interface

A rigorous definition of the ideally polarised interface is 'a system composed of a metal in contact with an electrolyte solution for which, at equilibrium, the concentration of every charged component is finite [ie. non-zero] in one phase only' [5]. The system will only be considered at equilibrium when, from the definition, no electrodic reaction occurs. Experimentally, the ideally polarised interface behaves like an electrical capacitor with no charge leakage. In practice this is never realised, but close approximations to it are possible. Such an interface can be considered as consisting of two phases of equal and opposite charge, $\pm\sigma_m'$, ie. as an electrical double layer[6]. Most of the charge is concentrated near to the interface so that the term excess charge is often used, referring to an excess compared with the bulk. At a molecular level the arrangement of the charged species is complex, particularly that of the electrolyte, and it is this which is of most interest here.

The structure of bulk electrolytes may be studied using

diffraction techniques, but unfortunately it is not yet possible to carry out similar experiments on the metal-electrolyte interface. The quantities most often observed for these latter systems are thermodynamic properties, such as interfacial tension, differential capacitance, surface excesses, etc. All these properties depend on σ_m' and on the charge distribution in the interface region. The approach we take is to start with a molecular model of the interface and compare, in particular, predicted capacitances with experimental ones for different values of σ_m' . A perfect description of the microscopic structure guarantees the accuracy of the predicted capacitance. Generally, a more realistic model is expected to give better agreement with experiment so that we may determine which features of the structure dominate the observed capacitance. However, this is not always true since it is possible for a relatively poor description of the structure to give good agreement with experiment because of fortuitous cancelling of errors.

As the charge of the two phases varies so does the potential drop, $\Delta\psi$, across the interface. Unfortunately, the absolute value of this quantity is not experimentally accessible. In practice, a second electrode must be used to provide a reference. This electrode is reversible and non-polarised and usually either the normal calomel or the hydrogen electrode is used. The experimental system is shown schematically in Figure 1.1. The applied voltage, V , across the interface will always be considered relative to the reference potential. Alternative symbols will be used to distinguish non-observable potentials.

It is convenient at this point to present the thermo-

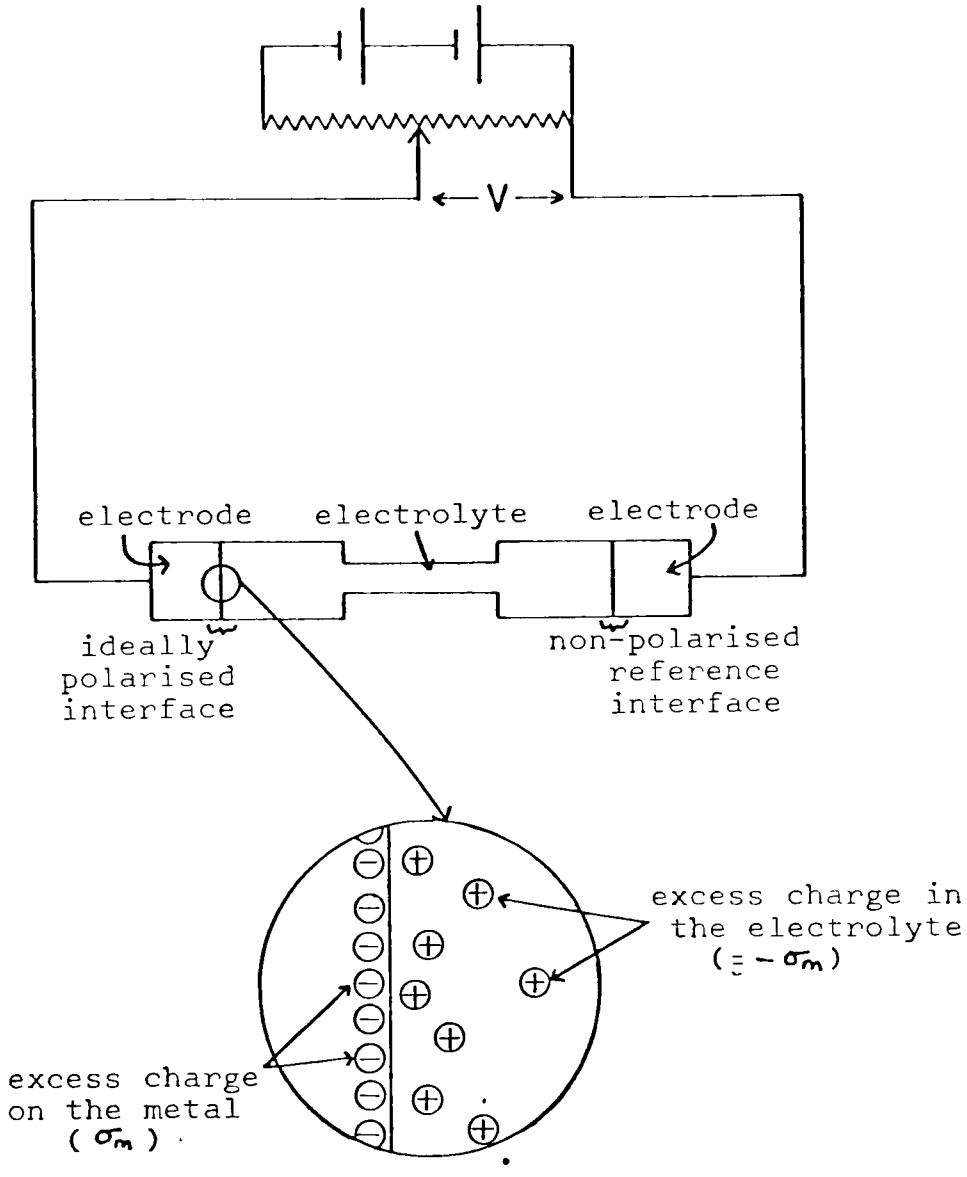


Figure 1.1 Schematic representation of the experimental system.

dynamics of ideally polarised interfaces used later. The first and second laws of thermodynamics give, for an open system[7]:

$$dU = TdS - dW - \sum_i \mu_i dn_i \qquad (1.1)$$

where U is the internal energy, T the temperature and S the entropy of the system and μ_i and n_i are the chemical potential and number of moles of species i. dW is the work done reversibly by the system which for an electrode-electrolyte interface is:

$$dW = pdV' + \gamma dA - V d\sigma_m' \qquad (1.2)$$

pdV is the work of volume expansion while γdA is the work of increasing the interface area, A, by dA with interfacial tension γ; $Vd\sigma_m'$ is the electrical work done when the charge on the electrode, σ_m', is changed. Since extensive properties are proportional to the size of the system, equation (1.1) may be written:

$$U = TS - PV' - \gamma A - V\sigma_m' - \sum_i \mu_i n_i \qquad (1.3)$$

Differentiating this equation and equating it to equation (1.1) with dW substituted using equation (1.2) gives, at constant temperature and pressure:

$$d\gamma = -\frac{\sigma_m'}{A} dV - \sum_i \frac{n_i}{A} d\mu_i \qquad (1.4)$$

This may be written in terms of the surface excesses, Γ_i:

$$d\gamma = -\sigma_m dV - \sum_i \Gamma_i d\mu_i \qquad (1.5)$$

where σ_m is the excess charge density on the electrode. For ideally polarised electrodes at constant composition equation (1.5) is reduced to:

$$\left(\frac{\partial \gamma}{\partial V}\right)_{\mu_i} = -\sigma_m \qquad (1.6)$$

which is the Lippmann equation[8]; it was originally derived without reference to the electrical double layer. It also holds for non-observable potentials[6], a property that will be used later. Equation (1.6) leads to a useful reference point namely, the point of zero charge (PZC) which occurs at the same applied potential as the maximum of the electrocapillary curve. Very different systems may thus be compared under similar conditions.

The electrified interface consists of two phases of equal and opposite charge. Most simply, the charge density of the metal, σ_m, can be considered to be on the metal surface and that of the electrolyte, $-\sigma_m$, on a plane parallel to the electrode and a distance, d, from it. Then the interface is analagous to a capacitor with an integral capacitance, K,[9]:

$$K = \frac{\sigma_m}{V} = \frac{\varepsilon}{4\pi d} \qquad (1.7)$$

where ε is the dielectric constant of the electrolyte. This capacitance is constant and independent of the applied potential. However, the observed capacitances of metal-electrolyte interfaces usually do vary with V and thus a differential capacitance is

defined[6]:

$$C \equiv \left(\frac{\partial \sigma_m}{\partial V}\right)_\mu = -\left(\frac{\partial^2 \gamma}{\partial V^2}\right)_\mu \tag{1.8}$$

where the second equality follows from equation (1.6).

Chapter 2 Theories of the hard wall-aqueous electrolyte interface

As we observed above, the physical system we wish to describe is the metal-electrolyte interface. In this chapter and the next we will be concerned particularly with aqueous electrolytes. In order to make progress with such a complex system we need first to consider simplified models which have some, but not all, of the features of the physical system. The success of the models in reproducing the results of experiments is expected to give an indication of the importance of these features in determining the behaviour of the actual system. Such considerations are left until Chapter 3 while in this chapter some of the more widely-used approximate theories of the electrified interface are presented. The results obtained by applying the theories to models of the interface are also given. They are compared with each other and with the ' experimental results ' obtained for the models from computer simulations. The model of the electrolyte used in many studies is the restricted primitive model[10] defined in section 2.2, while the electrode is represented as a charged hard wall.

Most of the theoretical studies of the interface fall into one of two main categories: those based on Gouy-Chapman theory[11, 12] and those based on integral equations of the statistical mechanics of fluids. The latter class may be further subdivided according to whether or not they are derived in terms of the direct correlation function of Ornstein and Zernike[13]. An example of a different approach is the layered lattice gas model proposed by Liu[14] and developed by Macdonald[15]. In all of these theories it is the physical features of the electrolyte which are emphasised

and until recently the effect of the nature of the metal on the properties of the interface was neglected. The role of the metal will be discussed in Chapter 5.

2.1 Gouy-Chapman theory and its extensions

Here, consideration of the bulk electrolyte is used as a starting point for the derivation of the Gouy-Chapman theory. It should be noted that originally it was derived without reference to the bulk[11,12]. The electrolyte is considered to be a continuum with dielectric constant ε, containing point ions carrying charges $z_j e$ and $z_k e$. The potential, $\phi(\underline{r})$, at a point $\underline{r}$ in such a medium is given by[9]:

$$\phi(\underline{r}) = \sum_i \frac{z_i e}{\varepsilon |\underline{r} - \underline{r}_i|} \qquad (2.1)$$

where the summation is over all the ions in the system. Keeping particle 1 fixed at, say, $\underline{r}_1$, the potential is averaged over all the configurations of the other particles giving the canonical average of the potential, $\langle \phi(\underline{r}, \underline{r}_1) \rangle_1$. The subscript indicates which particle has been fixed. This potential satisfies the Poisson equation[16]:

$$\nabla^2 \langle \phi(\underline{r}, \underline{r}_1) \rangle_1 = -\frac{4\pi}{\varepsilon} \langle \rho(\underline{r}, \underline{r}_1) \rangle_1 \qquad (2.2)$$

$\langle \rho(\underline{r}, \underline{r}_1) \rangle_1$ is the total charge density which may be written in terms of radial distribution functions:

$$\langle \rho(\underline{r}, \underline{r}_1) \rangle_1 = \sum_\alpha n_\alpha z_\alpha e \, g_{1\alpha}(\underline{r}, \underline{r}_1) \qquad (2.3)$$

where the summation is over the ion types. n_α is the bulk number concentration of α-type ions and $g_{1\alpha}(\underline{r},\underline{r}_1)$ is the radial distribution function of the same ions about the central ion at $\underline{r}_1$.

We now introduce the potential of mean force, $w_{1\alpha}(\underline{r},\underline{r}_1)$, which is defined by:

$$g_{1\alpha}(\underline{r},\underline{r}_1) \equiv e^{-\beta w_{1\alpha}(\underline{r},\underline{r}_1)} \tag{2.4}$$

where $\beta = 1/kT$, k being the Boltzmann constant. Using this equation and noting that $\phi(\underline{r},\underline{r}_1)$ and $g_{1\alpha}(\underline{r},\underline{r}_1)$ depend only on $|\underline{r}-\underline{r}_1|$ we obtain:

$$\nabla^2(\langle\phi(\underline{r})\rangle_1) = -\frac{4\pi e}{\varepsilon}\sum_\alpha n_\alpha z_\alpha e^{-\beta w_{1\alpha}(\underline{r})} \tag{2.5}$$

This is exact for the model system under consideration.

Equation (2.5) is the starting point for both Gouy-Chapman theory and the more well-known Debye-Huckel theory for bulk electrolytes[17]. To derive Gouy-Chapman theory we consider the central ion (particle 1) to be infinitely large so that it is equivalent to a planar hard wall. In this limit the potential and charge depend only on the perpendicular distance from the wall x with the wall placed at $x=0$. The dielectric constant of the wall is the same as that of the electrolyte in this theory as image forces are neglected[9].

A crucial approximation is now made namely, that the potential of mean force is equivalent to the electrical potential, $\psi(x)$:

$$W_{W\alpha}(x) = z_\alpha e \langle \phi(x) \rangle_1 \equiv z_\alpha e \psi(x) \tag{2.6}$$

where the subscript W denotes wall and the potential $\psi(x)$ is relative to $\psi(\infty)$, the potential in the interior of the electrolyte. $\psi(\infty)$ is set equal to zero. The corresponding Poisson equation is:

$$\frac{d^2\psi(x)}{dx^2} = -\frac{4\pi e}{\varepsilon} \sum_\alpha n_\alpha z_\alpha e^{-\beta z_\alpha e \psi(x)} \tag{2.7}$$

which, using the identity

$$\frac{d^2\psi(x)}{dx^2} = \frac{1}{2} \frac{d}{d\psi(x)} \left(\frac{d\psi(x)}{dx} \right)^2$$

and noting that in the interior of the solution $d\psi(x)/dx = 0$ and $\psi(x) = 0$, may be integrated once:

$$\left(\frac{d\psi(x)}{dx} \right)^2 = \frac{8\pi kT}{\varepsilon} \sum_\alpha n_\alpha \left(e^{-\beta z_\alpha e \psi(x)} - 1 \right) \tag{2.8}$$

The left hand side of equation (2.8) may be rewritten using Gauss' law[9]:

$$\frac{d\psi}{dx} = \frac{4\pi}{\varepsilon} \sigma_S \tag{2.9}$$

where $\sigma_S = \int_0^\infty \langle \rho(x) \rangle_1 dx$. σ_S is thus the charge density per unit area of a cylinder of solution extending from the hard wall to the bulk of the solution. Because of charge neutrality, $\sigma_S = -\sigma_M$. Combining equations (2.8) and (2.9) gives:

$$\sigma_M = \sqrt{\frac{\varepsilon kT}{2\pi} \sum_\alpha n_\alpha \left(e^{-\beta z_\alpha e \psi(x)} - 1 \right)} \tag{2.10}$$

which for a z-z electrolyte (ie. $\alpha=1,2; z_1=-z_2=z$) simplifies to:

$$\sigma_m = 2\left(\frac{\varepsilon kTn}{2\pi}\right)^{\frac{1}{2}} \sinh\left(\frac{ze\psi(0)}{2kT}\right) \qquad (2.11)$$

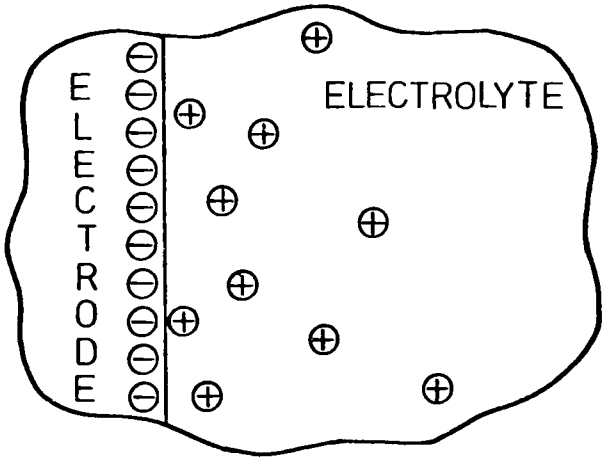
$\psi(0)$ is the potential at the metal surface relative to that of the bulk electrolyte and is equal to the external potential, V [18]. The charge on the metal surface may be related to the interfacial tension and the differential capacitance through equation (1.8):

$$\gamma = \gamma^{PZC} - \left(\frac{8\varepsilon k^2T^2n}{\pi z^2e^2}\right)^{\frac{1}{2}} \cosh\left(\frac{ze\psi(0)}{2kT}\right) \qquad (2.12)$$

$$C = \left(\frac{\varepsilon z^2e^2n}{2\pi kT}\right)^{\frac{1}{2}} \cosh\left(\frac{ze\psi(0)}{2kT}\right) = \frac{\varepsilon K_D}{4\pi} \cosh\left(\frac{ze\psi(0)}{2kT}\right) \qquad (2.13)$$

where γ^{PZC} is the constant of integration and K_D is the inverse Debye length[17].

The model of the interface used in Gouy-Chapman theory is obviously unphysical because the ions are considered as point charges. This assumption is not too serious for dilute electrolytes ($< .01M$[18]) but results in rather poor predictions for concentrations at which the ions occupy a significant volume (see Figure 3.1). The first, rather limited, inclusion of ion-size into the Gouy-Chapman theory was proposed by Stern in 1924[19]. In this model the point charges are no longer allowed to make direct contact with the wall, but have a finite distance of closest approach, x_{CA}, (see Figure 2.1), so resulting in two distinct regions: an ion-free region (usually referred to as the compact layer) and the remaining solution containing all the ions (the diffuse layer). Although the idea of a distance of closest approach is obviously linked with the idea of a finite ion size,



⊕ and ⊖ represent the excess charges of the two phases. The ions of the electrolyte are represented by point charges in both theories.

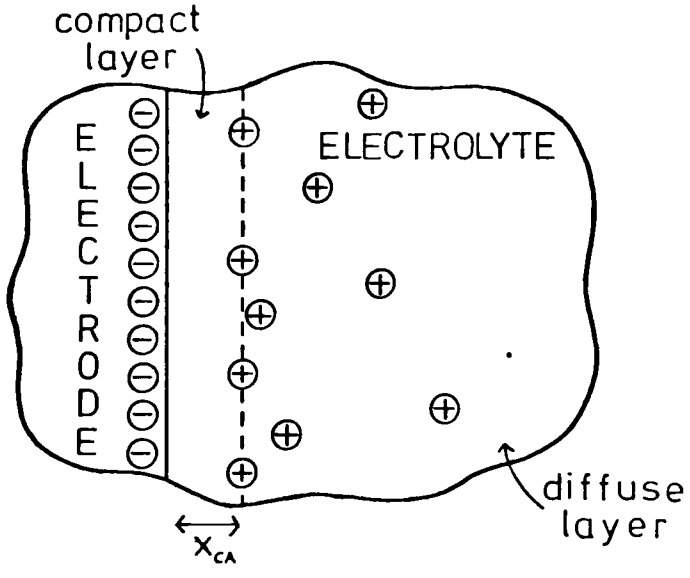


Figure 2.1 Relation between the Gouy-Chapman (top) and Gouy-Chapman-Stern theories.

this idea is not extended to the diffuse layer which continues to be described by Gouy-Chapman theory. The relations for the charge on the electrode and for the differential capacitance of the diffuse layer, C_d , become, for a z-z electrolyte:

$$\sigma_m = 2\left(\frac{\varepsilon kTn}{2\pi}\right)^{\frac{1}{2}} \sinh\left(\frac{ze\psi(x_{CA})}{2kT}\right) \qquad (2.14)$$

$$C_d = \frac{\varepsilon}{4\pi k_D} \cosh\left(\frac{ze\psi(x_{CA})}{2kT}\right) \qquad (2.15)$$

where $\psi(x_{CA})$ is the potential at $x=x_{CA}$ relative to that in the interior of the solution. In the Stern model the charge-free compact layer is equivalent to a parallel-plate condenser of dielectric constant ε so that it has an integral capacitance, K , (see equation (1.7)).

The differential capacitances, C_d and C_c , are simply related to the differential capacitance of the whole interface, C . The potential drop through the interface may be written as:

$$\Delta\psi = \psi(0) - \psi(\infty) = (\psi(0)-\psi(x_{CA})) + (\psi(x_{CA})-\psi(\infty)) \qquad (2.16)$$

which when differentiated with respect to σ_m :

$$\frac{\partial(\psi(0)-\psi(\infty))}{\partial\sigma_m} = \frac{\partial(\psi(0)-\psi(x_{CA}))}{\partial\sigma_m} + \frac{\partial(\psi(x_{CA})-\psi(\infty))}{\partial\sigma_m} \qquad (2.17)$$

and hence, using equation (1.8):

$$\frac{1}{C} = \frac{1}{C_c} + \frac{1}{C_d} \qquad (2.18)$$

This relation was first derived by Grahame[6]. It should be noted

that equation (2.18) is not specific to Gouy-Chapman-Stern (GCS) theory, but holds whenever the interface is split into two regions. Thus, it is used as a starting point in many theories designed to improve the description of one or both regions.

Recently, Valleau and Torrie[20] have made an obvious extension of GCS theory by including different distances of closest approach for each ion species and have calculated values of C_d for z-z electrolytes. Bhuiyan, Blum and Henderson[21] have made similar calculations for asymmetric, ie. z-z', electrolytes using the equations corresponding to (2.14) and (2.15) previously derived by Grahame[22]. There is little quantitative difference between the capacitances obtained from GCS theory and 'unequal radii' GCS theory. However, the inclusion of the two distances of closest approach introduces an asymmetry into the theoretical capacitance vs. potential (or charge) curves, a feature found in the experimental ones (see Figure 3.1).

There have been many attempts to improve upon other shortcomings of GCS theory, for instance, by including ions of finite size, a distance dependent dielectric constant, etc. These have been recently reviewed by Reeves[19]. The derivations are usually considerably more involved than that of the original theory for often little improvement of the results. One approach for which significantly different results are obtained is that of Outhwaite et al[23-25]. They included an ion volume term and a fluctuation term shown earlier by Kirkwood to have been neglected in the Poisson-Boltzmann equation for bulk electrolytes[26], so obtaining a 'Modified Poisson-Boltzmann' (MPB) equation. These authors made several different estimates of the first term and included image

terms in one calculation (see section 2.2). In common with most other extensions, the results approach those of the basic theory at low concentrations and surface charges.

2.2 Application of approximate integral equations to the interface region

In this section we take as the starting point the statistical mechanical theory of fluids and obtain approximate integral equations for the interface region. These equations are derived without reference to a molecular model of the interface, but in order to obtain results for a particular system, either analytically or numerically, they must be applied to such a model. This approach is in contrast with the Gouy-Chapman and GCS theories where the model is an integral part of the development of the theories. In fact, it is the starting point and the electrostatic and statistical mechanical relations are then written in terms of the model. The approaches involving integral equations have the advantage that they can be applied to different model systems, but because they are more general their derivations are much more involved than that of GCS theory. The resulting equations are also more complex and when they are applied to model systems it is usually only possible to obtain numerical results. For most models the GCS results are obtained as a low concentration limit.

Statistical mechanical quantities of great interest when studying fluids are the distribution functions, $g^{n}(r_1 \ldots r_n)$, where n is the order of the distribution function. Once these are known the thermodynamic properties of the system, in particular the capacitance, may be readily found. The general approach to obtain

$g^n(\underline{r}_1 \cdots \underline{r}_n)$ is to use one of the 'hierarchies' of distribution functions. These enable $g^n(\underline{r}_1 \cdots \underline{r}_n)$ to be written in terms of the next higher order distribution function (see, for example, Hansen and McDonald[27]). The distribution function of most interest when studying the interface is $g_{wi}(x)$ which gives the distribution of ions of type i as a function of x, the distance from the wall. $g_{wi}(x)$ is strictly a singlet distribution function, but the closed equations for it may be more simply derived if a pair distribution function, $g^2_{oi}(\underline{r}_1, \underline{r}_i)$, is considered in a limit when particle 0 is equivalent to a planar hard wall[28].

To gain a clearer idea of what is involved in the procedure to obtain $g^2(\underline{r}_1 \underline{r}_i)$ we now give an outline of the derivation of the Born-Green-Yvon (BGY) equation[29]. It has been simply derived for an electrified interface by Henderson et al[30]. Starting from the second equation of the BGY hierarchy they obtained, for an isotropic, one-component liquid:

$$-kT \bar{\nabla}_1 \ln g^2(\underline{r}_1, \underline{r}_2) = \bar{\nabla}_1 u(\underline{r}_1, \underline{r}_2) + n \int \frac{g^3(\underline{r}_1, \underline{r}_2, \underline{r}_3)}{g^2(\underline{r}_1, \underline{r}_2)} \bar{\nabla}_1 u(\underline{r}_1, \underline{r}_3) d\underline{r}_3 \qquad (2.19)$$

where n is the density, $g^3(\underline{r}_1, \underline{r}_2, \underline{r}_3)$ is the triplet distribution functions and $u(\underline{r}_1, \underline{r}_2)$ is the pair potential for particles 1 and 2. It has been assumed that the total potential energy of the system is pair-wise additive, ie:

$$U_N(\underline{r}_1 \cdots \underline{r}_N) = \sum_{i<j} u(\underline{r}_i, \underline{r}_j) \qquad (2.20)$$

Generalising equation (2.4) we can obtain the triplet distribution function in terms of the potential of mean force:

$$g(123) \equiv \exp\{-\beta w(123)\} \tag{2.21}$$

where the notation has been simplified in an obvious manner. A second approximation is now made namely, that this potential of mean force is pair-wise additive, ie:

$$w(123) \simeq w(12) + w(23) + w(31) \tag{2.22}$$

which implies that:

$$g(123) \simeq g(12)\,g(23)\,g(31) \tag{2.23}$$

This widely-used approximation is the superposition approximation of Kirkwood[31]. Using this approximation and considering the case of a mixture where particle 2 is extremely large (and so equivalent to a planar wall (suscript w)), Henderson et al obtained the BGY equation for a hard wall-liquid interface:

$$kT\frac{\partial \ln g_{wi}(x)}{\partial x} = \frac{\partial u_{wi}(x)}{\partial x} + 2\pi\sum_j \rho_j \int_0^\infty (x-s) g_{wj}(s)\,ds \int_{|x-s|}^\infty \frac{\partial u_{ij}(t)}{\partial t} g_{ij}(t)\,dt \tag{2.24}$$

$\rho_j g_{wj}(x)$ is the density profile of species j with x measured from the wall, $g_{ij}(t)$ is the bulk radial distribution function which can be obtained from the bulk BGY equation or from experiment and $u_{wi}(x)$ is the direct interaction of species i with the wall.

An alternative way of obtaining $g^2(r_1, r_2)$ is by using approximate forms for the direct correlation function, $c(r_1, r_2)$, defined by the Ornstein-Zernike equation:

$$h(r_1, r_2) = c(r_1, r_2) + \rho \int c(r_1, r_3)\, h(r_2, r_3)\, dr_3 \tag{2.25}$$

where $h(\underline{r}_1,\underline{r}_2)\,(=g(\underline{r}_1,\underline{r}_2)-1)$ is the total correlation function. $c(\underline{r}_1,\underline{r}_2)$ may be thought of as the 'direct' part of $g(\underline{r}_1,\underline{r}_2)$ [16], ie. the part involving direct physical interactions between **1** and **2**, so that:

$$c(\underline{r}_1,\underline{r}_2) = g_{total}(\underline{r}_1,\underline{r}_2) - g_{indirect}(\underline{r}_1,\underline{r}_2) \qquad (2.26)$$

Using the definition (2.21) and the approximation (2.20), equation (2.26) may be rewritten:

$$c(\underline{r}_1,\underline{r}_2) \simeq e^{-\beta w(\underline{r}_1,\underline{r}_2)} - e^{-\beta[w(\underline{r}_1,\underline{r}_2)-u(\underline{r}_1,\underline{r}_2)]} \qquad (2.27)$$

Substituting this into the Ornstein-Zernike equation gives the Percus-Yevick equation[32]:

$$e^{\beta u(\underline{r}_1,\underline{r}_2)}\, g(\underline{r}_1,\underline{r}_2) = 1 + n\int (1-e^{\beta u(\underline{r}_1,\underline{r}_3)})\, g(\underline{r}_1,\underline{r}_3)(g(\underline{r}_2,\underline{r}_3)-1)\,d\underline{r}_3 \qquad (2.28)$$

If the second term of equation (2.27) is first expanded:

$$c(\underline{r}_1,\underline{r}_2) \simeq e^{-\beta w(\underline{r}_1,\underline{r}_2)} - 1 + \beta[w(\underline{r}_1,\underline{r}_2)-u(\underline{r}_1,\underline{r}_2)] \qquad (2.29)$$

the Hypernetted Chain equation results[33]:

$$-\beta[w(\underline{r}_1,\underline{r}_2)-u(\underline{r}_1,\underline{r}_2)] = n\int\{(g(\underline{r}_1,\underline{r}_3)-1)+\beta[w(\underline{r}_1,\underline{r}_3)-u(\underline{r}_1,\underline{r}_3)]\}\, g(\underline{r}_2,\underline{r}_3)\,d\underline{r}_3 \qquad (2.30)$$

As written equation (2.30) is for a one-component, isotropic, bulk liquid, but the corresponding equation for the hard wall—liquid interface may be fairly readily obtained[34].

The mean spherical approximation[35], which is frequently

used to describe the electrolyte, also involves the Ornstein-Zernike equation, but unlike the integral equations already mentioned it is for a particular model. This approximation is discussed further in Chapter 4. Lastly, $g_{wi}(x)$ is often obtained using the mathematically convenient exponential approximation[36]. A brief derivation of this is given in Appendix D.

The differential capacitance of the diffuse layer is essentially obtained by integrating the charge distribution over the distance from the wall. $g_{wi}(x)$ may be obtained from equation (2.24) and appropriate forms of equations (2.28) and (2.30) once a choice of interaction potential has been made. Ideally, this would be the exact form for the physical system but, since this is not known, an approximate interaction potential must be used. Aqueous electrolytes are most often represented by the restricted primitive model[10] in which the electrolyte is considered as a continuum dielectric containing hard spheres of equal diameters, d, and with charges $\pm ze$. The interaction potential between the ions is given as a sum of pair potentials, each of the latter being a combination of an infinite hard sphere repulsion and a Coulomb tail:

$$u_{ij}(r) = \infty \qquad r < d$$
$$= -\frac{z^2e^2}{\varepsilon r} \qquad r \geq d \tag{2.31}$$

The metal electrode is usually modelled as a charged hard wall of the same dielectric constant and thus $u_{wi}(x)$ is given similarly.

For any given model interface, the results for $g_{wi}(x)$ from the approximate integral equations are qualitatively similar but they do differ, particularly near to the hard wall. For the

charged hard wall-charged hard spheres system Henderson et al[37,38] have derived an exact equation for the contact values of $g_{wi}(x)$ which for a z-z electrolyte is:

$$nkT\left[g_{w1}(d_1/2) + g_{w2}(d_2/2)\right] = P + \frac{\varepsilon}{8\pi}\left(\nabla\psi(0)\right)^2 \qquad (2.32)$$

where P is the pressure of the bulk electrolyte. The BGY equation satisfies this condition exactly[30,39]. The HNC and Modified Poisson-Boltzmann (MPB) equation satisfies equation (2.32) fairly well, but the MSA and GCS underestimate the contact values[25,37]. For a wider assessment of the accuracy of a theory applied to a model, experimental data for the model is required. This is obtained from computer simulation of the interface. Very recently, Valleau et al and van Megen and Snook extended their Monte Carlo work on bulk electrolytes[40-44] to the interface region[45-48]. In most cases the restricted primitive model was studied near a charged hard wall with no account of image forces being taken. The 'experimental data' may be compared with the numerical results for the theories applied to similar models. Unfortunately, in practice direct comparison is often not possible because the hard spheres of the restricted primitive model have been given different diameters in the theoretical studies compared with the 'experimental' ones. However, since the Monte Carlo results have been available the parameters used to obtain these have also been used in the theoretical studies.

In Figure 2.2 we have collected the results for the variation of $\psi(x_{CA})$, the potential at x_{CA}, with σ_m from several theoretical and 'experimental' studies[37,48,49] which are directly

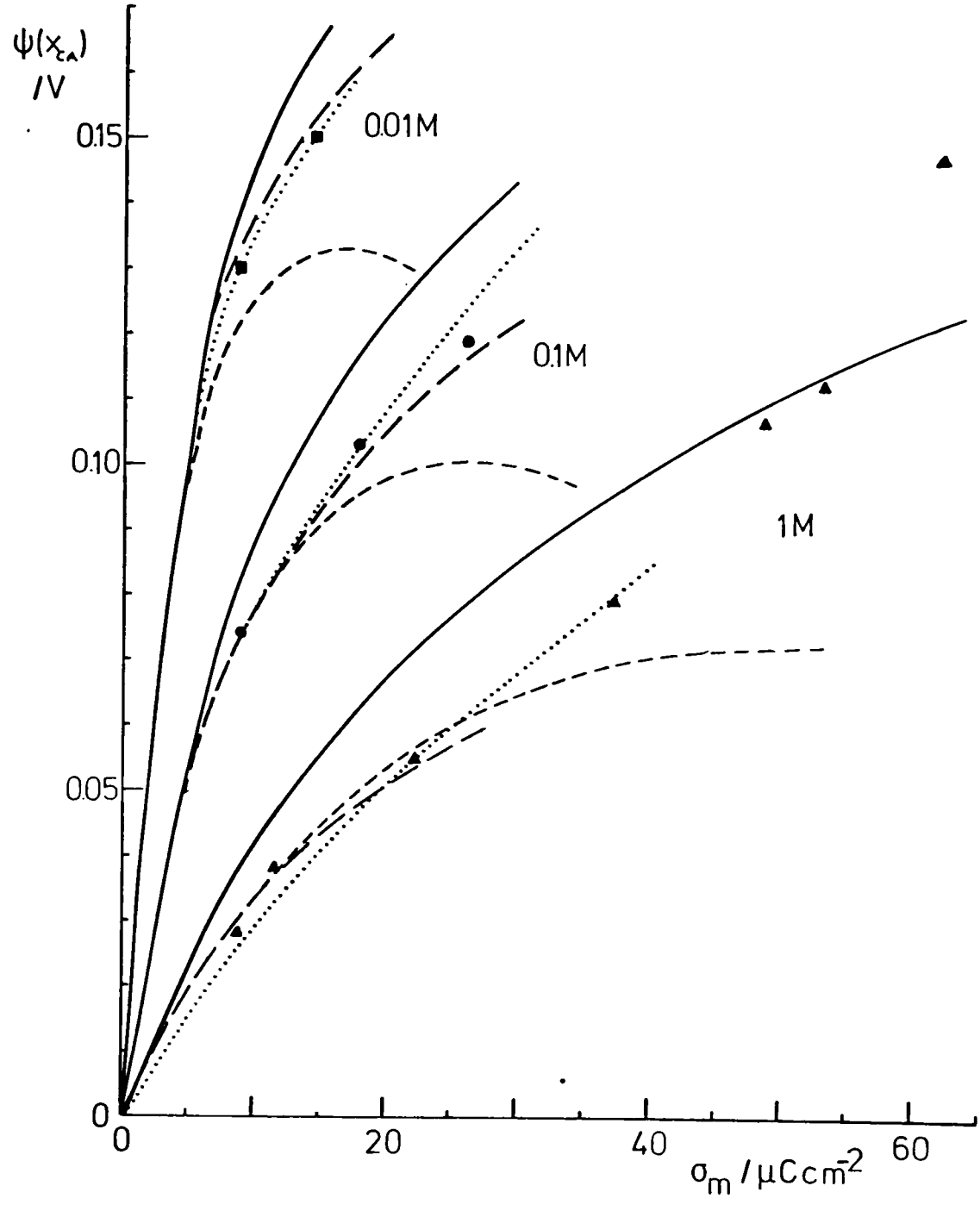


Figure 2.2 $\psi(x_{cA})$ as a function of metal charge density; solid points Monte Carlo results; ——MCC, ·····MPB, – – – HNC, — — HNC/MSA. All the curves correspond to $x_{cA} = d/2 = 2.125$Å, $z = 1$, $T = 298$K and $\varepsilon = 78.5$.

comparable. The values for GCS theory were calculated from equation (2.15). Although the HNC approximation gives good values for the contact values of the ion distributions, it gives $\psi(x_{CA})$ poorly. Most significantly it predicts the variation of $\psi(x_{CA})$ to be non-monotonic with charge, a feature absent from the simulation. GCS theory predicts the monotonic behaviour but overestimates $\psi(x_{CA})$. This is corrected for by the MPB equation which from Figure 2.2 appears to be very successful. In addition, comparison of one form of the equation which includes some account of image effects with simulation results for a model also including these effects shows that there is close agreement between the two[50]. However, for 1-2 electrolytes the MPB equation predicts non-monotonic behaviour for $\psi(x_{CA})$ [51] and, for higher concentrations ($\geq$ 2M), its ion distribution functions are highly dependent on the estimate of the volume term used[24,25,48] (see section 2.1).

Values obtained by applying the HNC/MSA theory to the interface are also given in Figure 2.2. In this approximation the wall-ion distribution functions are given by the HNC theory while those of the bulk are given by the MSA. It is more successful at higher charges than the HNC approximation, but values of $\psi(x_{CA})$ are only available for a limited range of σ_m. Also the HNC/MSA approximation underestimates the density of co-ions (ie. those with charge of the same sign as σ_m) near the wall. Finally, Croxton and McQuarrie[39] have recently calculated $\psi(x_{CA})$ and $g_{wi}(x)$ values using the BGY equation. Direct comparison with the simulation results is not possible because different parameters were used in the two cases. However, there is qualitative agreement.

Figure 2.3 shows the variation of the differential capacitance with applied potential as predicted by several theories [37]. MEXP is a modification of the exponential approximation which satisfies local charge neutrality. The capacitance of the model system from computer simulation has not been calculated. It can be seen from Figure 2.3 that the predicted results become similar at low concentrations and applied potentials. This is generally true of the results of the approximate theories and they tend to the GCS theory values. In some cases the relation with the latter theory may be shown analytically, for example for the HNC approximation[34].

In summary, then, it may be concluded that results in reasonable agreement with those of computer simulations of the charged hard wall-charged hard spheres system are obtained using several different approximations. The approaches used vary significantly in complexity, but there is little to choose between the final results. There is closest agreement with the simulation values at low concentrations and surface charges.

In a small number of studies of the interfacial region the electrolyte has been modelled more realistically by considering both the ions and the solvent as discrete particles. This work is discussed in some detail in section 3.3.

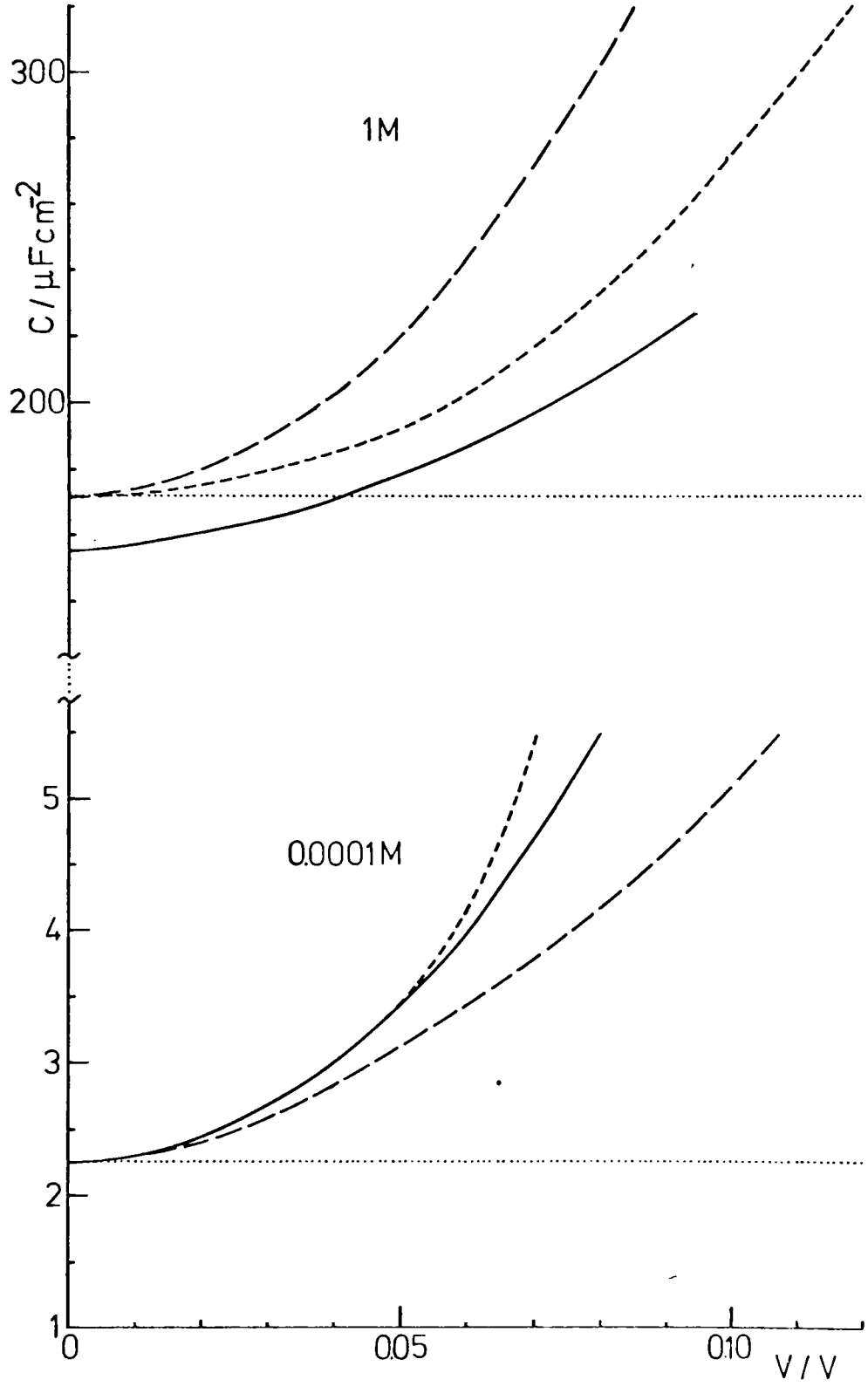


Figure 2.3 Differential capacitance as predicted by GCS theory (———) and the MSA (·····), EXP (– – –) and MEXP (– · – · –) approximations. The model parameters are d 2.7Å°, z = 1, T = 298K and ε 78...

Chapter 3 Comparison of theoretical and experimental results for metal-aqueous electrolyte interfaces

There is one significant criticism that can be made of the work discussed in Chapter 2. This is the general lack of attempts to relate the results of the theories to the experimental ones. There are two points to be considered in connection with this. First, the quantities of interest to most theoreticians are either not experimentally accessible, for example $\psi(x_{c_1})$ (see Figure 2.2), or else may only be obtained with difficulty. $g_{wi}(x)$ is such a quantity since structural measurements pose much more of a problem for metal-electrolyte interfaces than for bulk electrolytes. Indeed no such measurements for these interfaces are known to us.

The second point is that although much theory and formalism has been developed this has usually been applied to simplified models of the interface so that it may not be meaningful to compare the two sets of results. This certainly seems to be the view of most workers who use integral equation approaches. They have concentrated on obtaining agreement between the theoretical predictions and computer simulation results for the idealised models without reference to the, rather different, experimental results. This view does not seem entirely justified as models are introduced to allow a better understanding of the more complex physical system. Comparison of the theoretical and experimental results should therefore be made as the model which includes the dominant features of the physical system is likely to yield the closest agreement with experiment.

However, the capacitance calculated using equation (2.18) may be compared with experimental values (section 3.2). From su

a comparison it is clear that in general the combination of a parallel plate capacitor model for the compact layer and a description of the diffuse layer using any of the theories of Chapter 2 cannot predict the experimental capacitances. As the discussion in section 3.2 shows one of the most important features of the physical system omitted in the models of Chapter 2 is the structure of the solvent in the compact layer. Many experimentalists realised this and have subsequently tried to incorporate this feature although usually without much formal theoretical justification. We discuss some of these attempts in section 3.3.

3.1 The experimental system

Most of the experimentally observable properties of metal-aqueous electrolyte interfaces are thermodynamic ones, measurement of the structural features of interfaces being difficult. Here we are mainly concerned with the differential capacitance but it is useful also to consider the interfacial tension, γ. Early experimenters, in particular Gouy[52] and Frumkin[53], concentrated on measuring γ by means of an ellipsometric technique suggested by Lippmann[8]. More recently, the trend has been towards measuring the differential capacitance using ac bridge methods. For a critical review of modern experimental methods see Habib and Bockris[54]. The two measured quantities are related through equation (1.8). However, in many cases there is some discrepancy between the measured and derived values (of either quantity). This is because the interfaces are not close to being ideally polarised ones and thus the thermodynamics of section 1.1 does not hold exactly. This does not concern us here since we have chosen to consider only systems which contain approximate ideally polarised

interfaces namely, mercury-aqueous electrolyte systems. In addition they are systems for which the experimental data is in general very reliable[54].

A wide variety of electrified interfaces has been studied and, apart from that between metal electrodes and aqueous electrolytes, there have been experiments on colloidal systems, systems with semi-conductor or insulator electrodes and those with other electrolytes such as non-aqueous electrolytes and molten salts. In this chapter we will restrict consideration of the experimental systems to mercury-aqueous electrolyte interfaces because our aim is to discover how well theoretical predictions compare with experimental results. The models used are essentially physical ones with the interactions arising from Coulomb forces and hard-sphere repulsions. The metal and solvent are included as continuums and different ionic species are only represented by different hard sphere diameters. With such little account being taken of chemical factors we cannot expect the models to predict the differences observed on changing the chemical nature of the system. Thus, we consider only a restricted group of interfaces and concentrate on the dependence of their properties on the experimental conditions such as applied potential, temperature and electrolyte concentration.

Apart from the thermodynamic reasons, mercury-aqueous electrolyte interfaces were chosen for study as there is a relatively large amount of data for these systems. Initially, mercury was used predominantly because ellipsometry requires a liquid metal and at room temperatures Hg exists in this state. More modern techniques allow the use of solid electrodes, but until very

recently measurements for these were not reproducible because of contamination of the electrode surface[54]. Contamination of liquid metals is minimal as for these a dropping electrode[55] may be used in which the electrode is frequently replaced. This technique has mainly been used with mercury, although there have been some applications to gallium and various amalgams by Russian researchers[56]. A final reason why mercury is preferred is because the mercury-solution interface is approximately ideally polarised over an unusually wide range of applied voltage (~2V)[1].

3.2 Comparison of predicted and experimental capacitances

3.2.1 The magnitude of the capacitance

Experimental capacitance versus applied potential curves for metal-aqueous electrolyte systems typically have two minima separated by a maximum[57], althcugh one or more of these turning points may not be observed at low concentrations and high temperatures. Gouy-Chapman theory, however, predicts a parabolic variation with the minimum at V^{pzc}. Better results may be obtained by including a compact layer contribution with the resulting total capacitance given by equation (2.18), and this has been done for the Hg-aqueous NaF system[58,59] (see Figure 3.1). In Figures 3.1 (b) & (c) a pronounced minimum near V^{pzc} can be seen in the experimental curves. This is one indication that there is little specific adsorption[6,54] - when some electrolyte ions are in direct contact with the metal (see section 3.3) - and it is for this reason that NaF was chosen. When there is no specific adsorption the compact layer is charge free so that its capacitance is independent of electrolyte concentration. Assuming this to be the

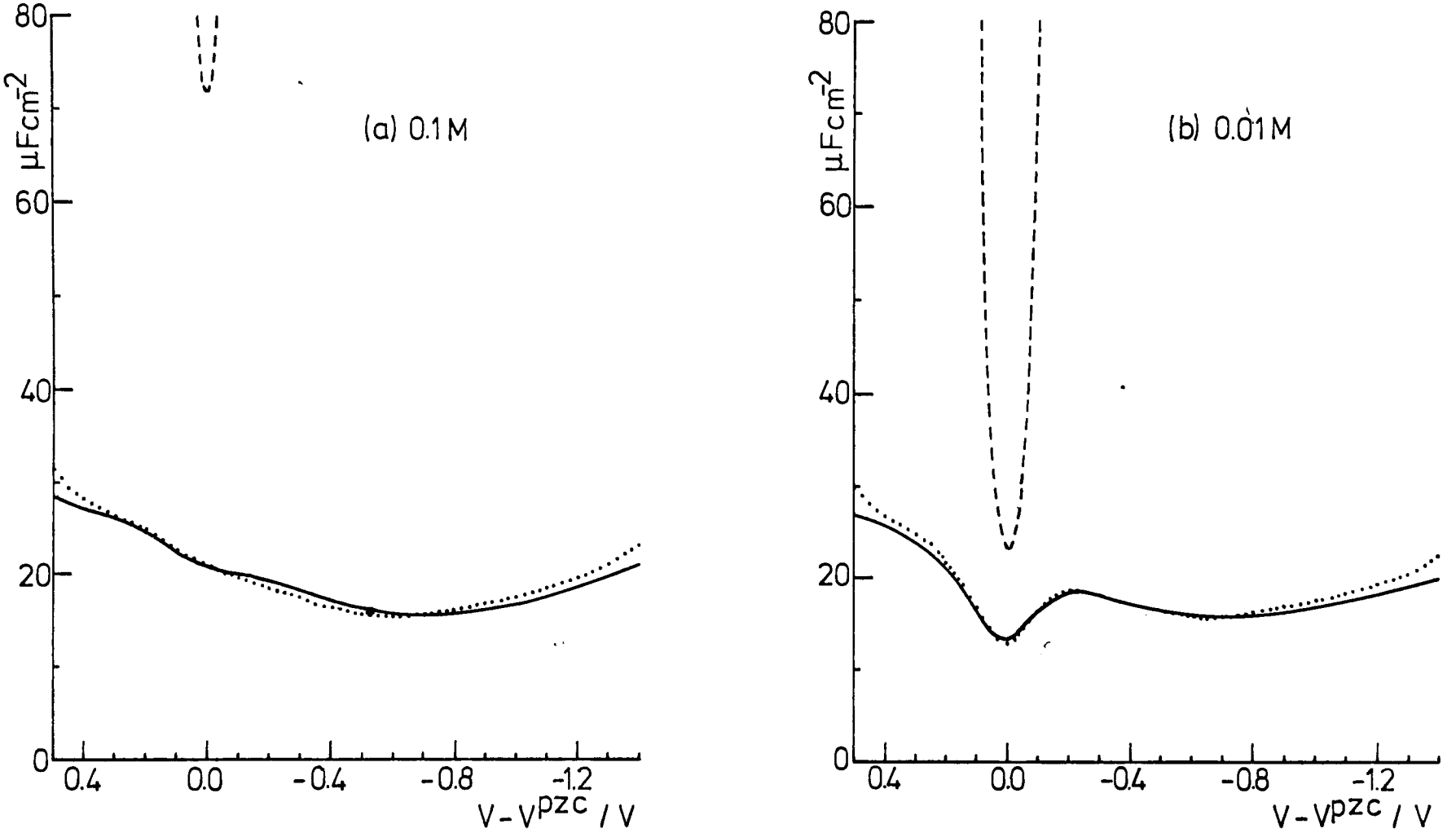
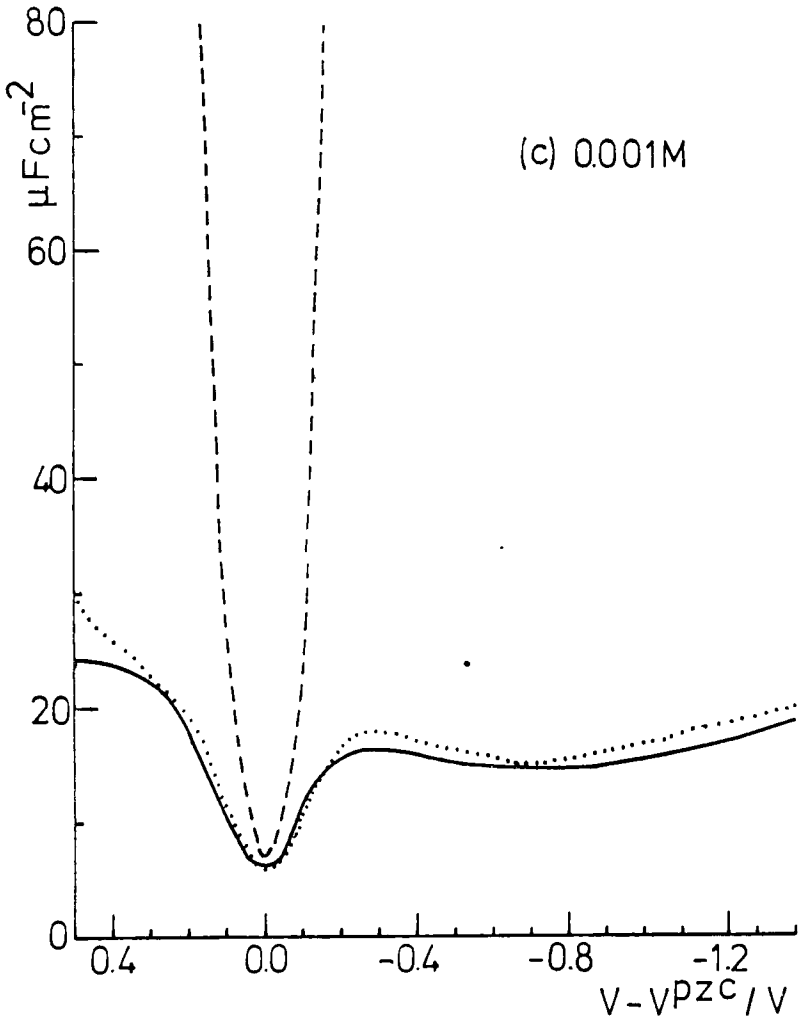


Figure 3.1 Experimental capacitance values (——) for the Hg-aqueous NaF system at 4 electrolyte concentrations together with values predicted by Gouy-Chapman theory (- - - -) and calculated from equation (2.18) (·····) (see text).



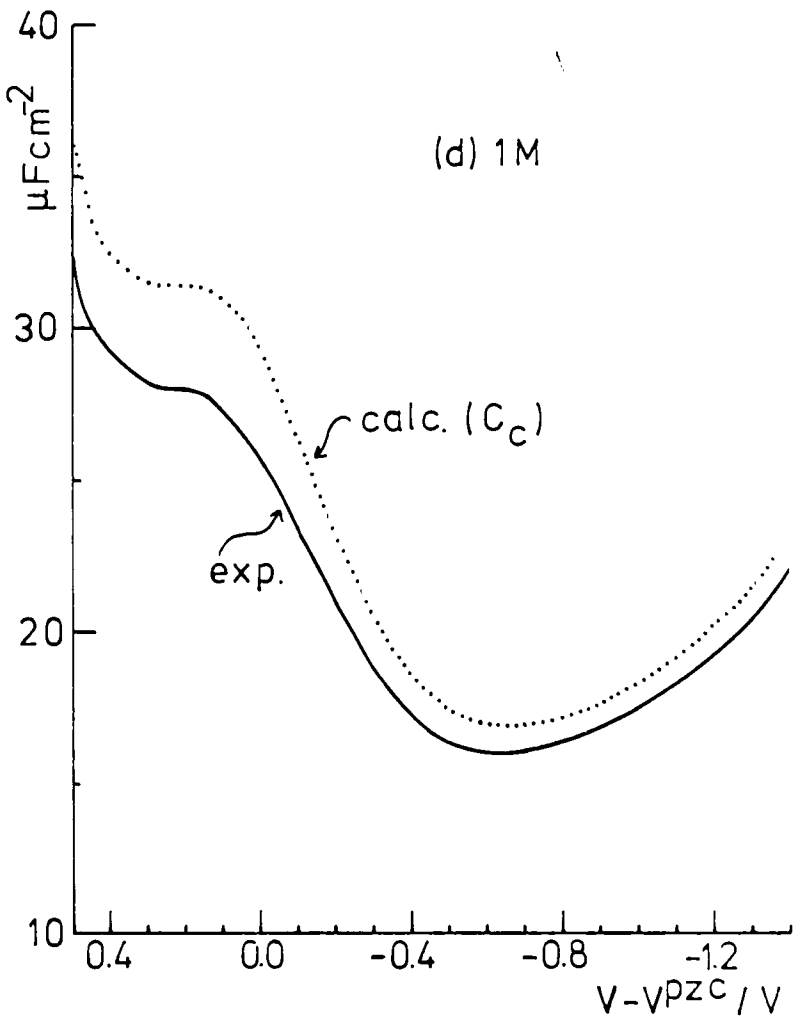


Figure 3.1 continued

case the capacitances were calculated for three concentrations using the compact layer capacitance calculated from data for 1M NaF (Figure 3.1(d)). The values obtained are in good agreement with the experimental ones.

As may be seen from Figure 3.1 (a)-(c), Gouy-Chapman theory gives poor results except at low concentrations and applied potentials. It is also clear that at most concentrations and applied potentials the contribution of the diffuse layer to the capacitance of the physical system is relatively unimportant compared with that of the compact layer. However, it is the diffuse layer which is described in detail by the theories of Chapter 2 while the compact layer is usually considered as a parallel plate capacitor with a constant capacitance. Such a combination of descriptions of the two layers cannot give the observed capacitances even for a charge free compact layer as is clear from Figure 3.1 (d). This indicates that the solvent has an important role in the compact layer which is not being included in the theories of Chapter 2. Specific adsorption, which occurs in most systems of interest, also affects the compact layer capacitance. Because of the importance of this contribution to the experimental capacitance it may be concluded that without a better theory of the compact layer there is little point in having such detailed ones for the diffuse layer. A fuller discussion of the compact layer is given in section 3.3.

3.2.2 The concentration and temperature dependence of the capacitance

As seen from Figure 3.1., Gouy-Chapman theory gives reason-

able results for the capacitance of Hg-aqueous NaF systems at low concentrations and applied potentials. NaF is a particularly favourable case as there is little specific adsorption, but the theory does best in the same region for other systems, although the results are poorer over the whole potential range. For this reason we look here particularly at the capacitance at the point of zero charge, C^{pzc}, which in Gouy-Chapman theory is given by (from equation (2.13)):

$$C^{pzc} = \left(\frac{\varepsilon z^2 e^2 n}{2\pi kT}\right)^{\frac{1}{2}} \qquad (3.1)$$

We already have a good idea of how well Gouy-Chapman theory predicts the concentration dependence of C^{pzc}. From the derivation of the theory and Figure 3.1 it may be concluded that the theory is correct in the limit of low concentration, but that the predicted values become too high as the concentration is increased. In Figure 3.2 results for several Hg-aqueous electrolyte systems are given[61-72] together with the Gouy-Chapman result. This figure confirms our conclusion for high concentrations but shows that when there is significant specific adsorption (for example KBr, KI) the theory does not give the correct values even in the low concentration limit.

There have been relatively few studies of the temperature dependence of the capacitance and in addition the results of these studies have been published usually only as small figures so making it difficult to reproduce them. It is clear however, that the general form of the capacitance curves changes as the temperature is varied. For aqueous electrolytes the maximum disappears

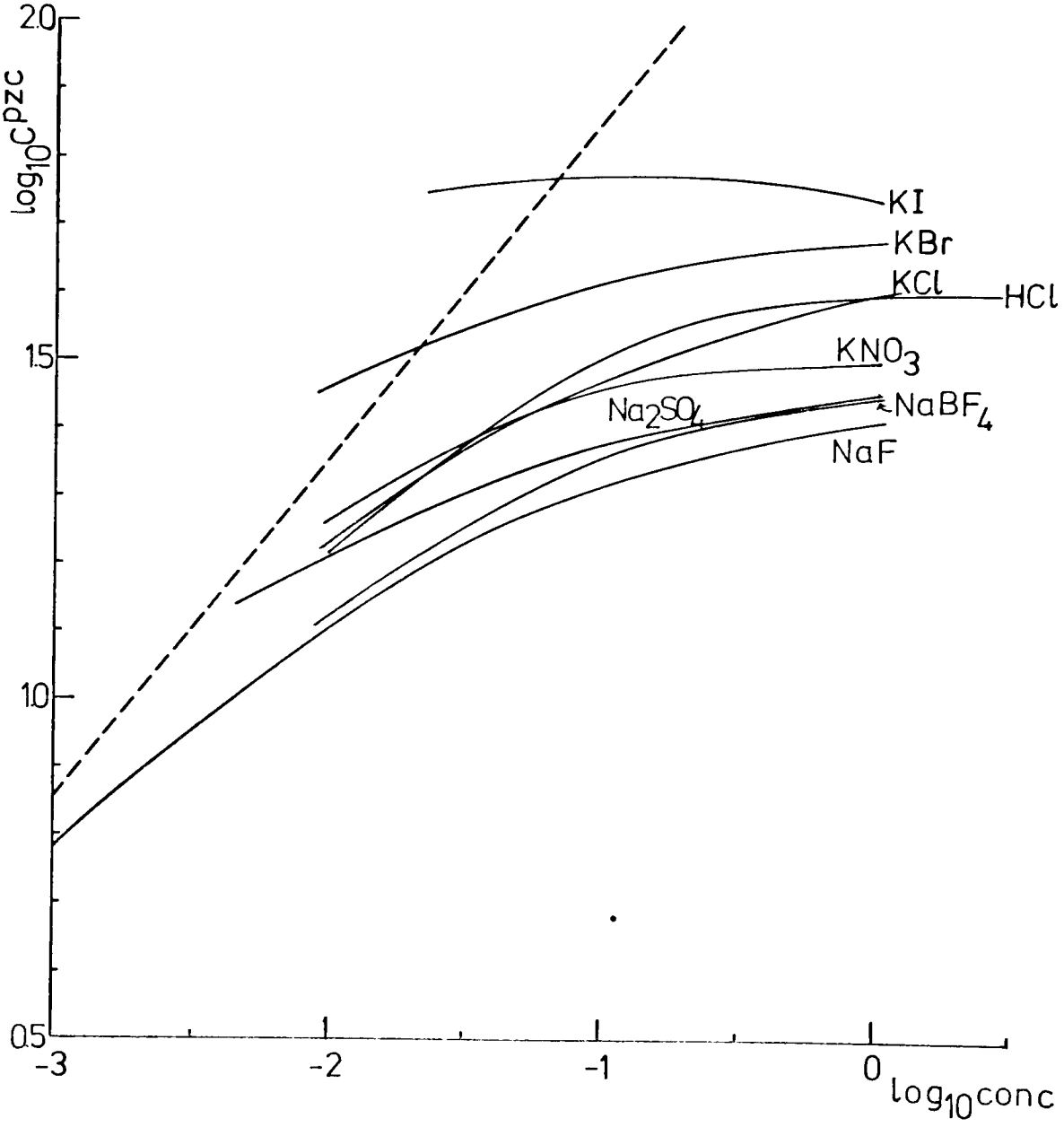


Figure 3.2 Variation of C^{pzc} with electrolyte concentration for various aqueous electrolytes. The dashed line is the Gouy-Chapman result.

as the temperature is raised while the minimum at the more negative applied potential remains essentially unchanged. At the PZC the capacitance decreases with temperature and for most of the systems studied the dependence is close to that predicted by Gouy-Chapman theory (see Figure 3.3[67,73-77]). Several authors, in particular Buhl[77,78] and Grahame[76,79], have given qualitative explanations of the temperature dependence of the capacitance curves in terms of the structure of water at the interface and in terms of specific adsorption. Thus, again we must conclude that the compact layer is dominant in determining the observed properties of the electrified interface.

3.3 The compact layer

The comparison of theoretical and experimental capacitance curves given in the last section makes it clear that at most applied potentials and electrolyte concentrations ($>$ .001M) the major contribution to the capacitance of the metal-aqueous electrolyte interface comes from the compact layer. Diffuse layer theory gives the qualitatively correct temperature dependence of C^{PZC} but it is not successful away from this point. In addition it does not explain the dependence on electrolyte concentration. Thus, in order to bring the theoretical results into closer contact with the observed measurements it seems likely that inclusion of the compact layer is required. In Gouy-Chapman-Stern theory the compact layer is modelled as a parallel plate condenser so that it has a constant capacitance as the applied potential is varied. This model has two serious short-comings: the solvent is included only as a continuum medium and not at a molecular level and only electrostatic interactions are included with no account of chemical

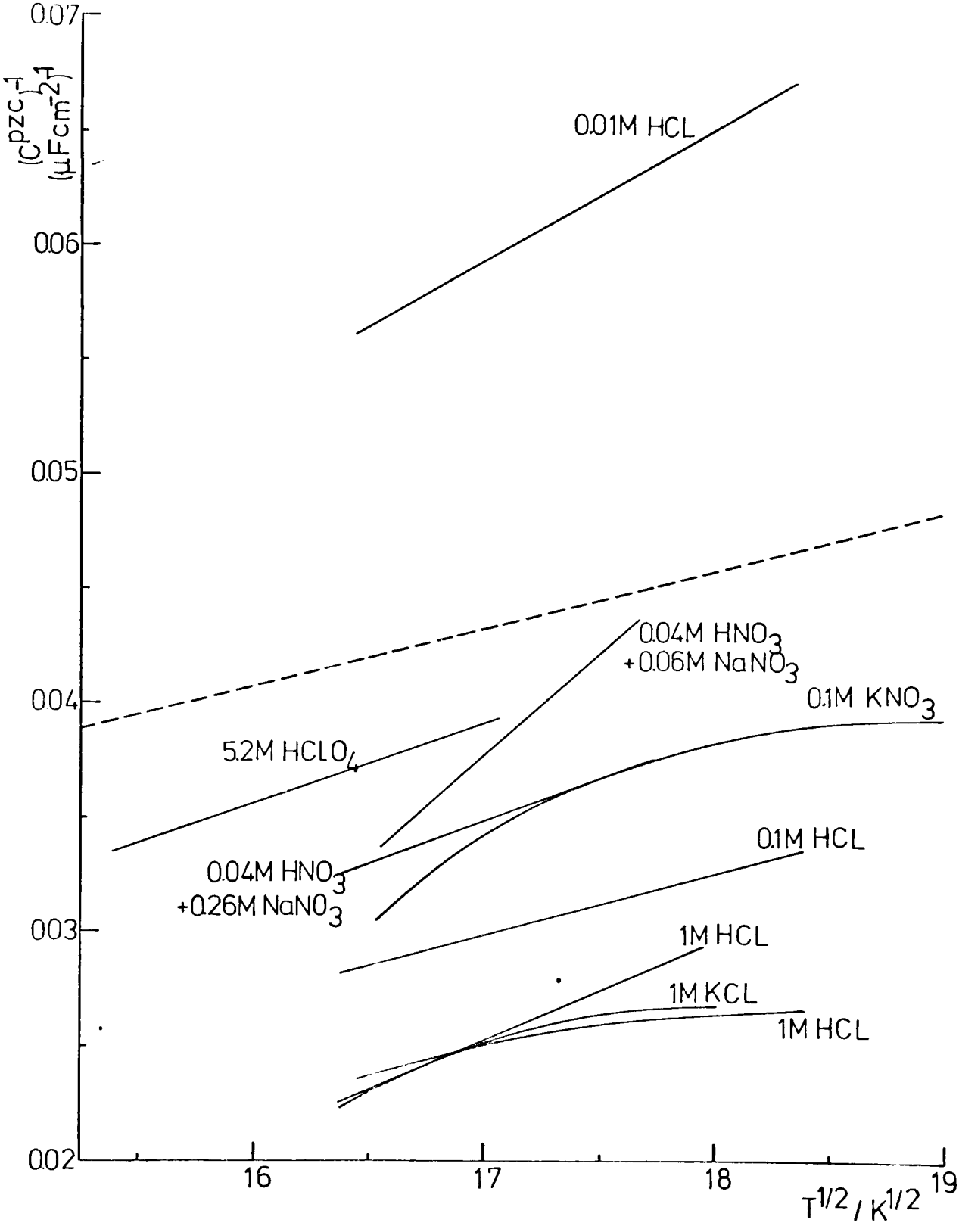


Figure 3.3 Variation of C^{pzc} with temperature for various aqueous electrolytes. The dashed line is the Gouy-Chapman result.

interactions. There have been many attempts to improve upon both of these aspects of the model[1,54] and a brief discussion of some of the more successful ones is given below.

Consider first the solvent. A model in which the charge free compact layer is represented as a layer of dipoles should be an improvement on the continuum model. In such models, as first suggested by Trasatti[80], the potential drop across the compact layer is split into two contributions:

$$\Delta\psi_c = \psi(0) - \psi(x_{CA}) = \psi_{ion} + \psi_{dipole} \qquad (3.2)$$

where ψ_{ion} arises from the presence of charge on the metal surface and in the diffuse region while ψ_{dipole} is associated with the dipoles. Using equation (1.8) and remembering that there must be overall charge neutrality, the compact layer capacitance is found to be:

$$\frac{1}{C_c} = \frac{1}{C_{ion}} - \frac{1}{C_{dipole}} \qquad (3.3)$$

By assuming that the molecular polarisability of the solvent is a constant isotropic property, C_{ion} becomes an integral capacity which may be easily evaluated. This leaves C_{dipole}. C_{dipole} has been modelled in two ways. In the first approach a molecular model of the solvent is proposed. General theories are then applied to this model leading to predictions which can be compared with experimental data. The predicted curves have a functional form with parameters hopefully of physical significance. Secondly, the experimental data is used as a starting point and parameters are derived this time from simple assumptions without the model for

a molecular model a priori. An example of this approach is the work by Trasatti on water orientation at metal surfaces[81,82]. This is discussed in Chapter 5.

The first route for obtaining C_{dipole} has been by far the more popular and the basis for most recent modelling came from Watts-Tobin[83] who proposed that the solvent dipoles in the compact layer could be modelled as being in one of two states: pointing towards or away from the metal surface. Such two-state models fail to account for the asymmetry in the experimental capacitance curves. More recently, Fawcett[84] has shown that such a feature can be predicted by invoking a three-state model which includes in addition to the former two states a third in which the dipoles are parallel to the metal surface. By estimating the non-electrostatic contributions to the interaction energy Fawcett also included some of the chemistry of the experimental systems. It can be seen from Figure 3.4 (a) & (b), where the experimental and theoretical C_c vs. σ_m curves are shown for ethylene carbonate and methanol, that there is good agreement between the two. The relative proportions of the three possible states for the solvent dipoles are also shown.

There are, however, some limitations of Fawcett's three-state model, the most important of which for the present discussion being that poor results are obtained when there is a significant degree of association between the solvent molecules as is the case for water[85]. In such solvents clusters consisting of two or three molecules exist and these have a smaller net dipole moment than a single isolated molecule. This limitation of the three-state model can be seen in Figure 3.4 (b) where the theoretical and experimental curves for methanol diverge as σ_m becomes positive. Fawcett[86]

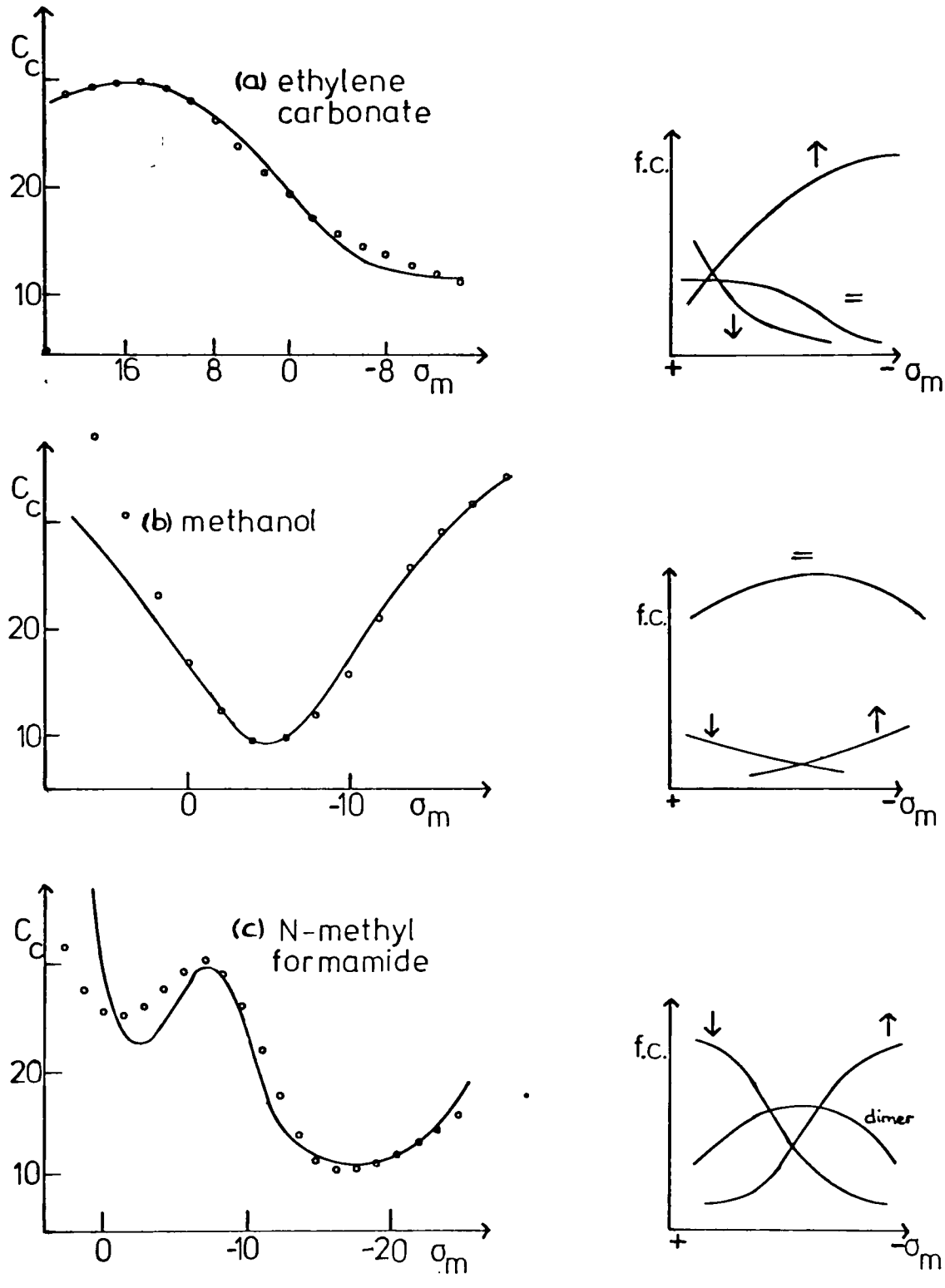


Figure 3.4 Experimental compact layer capacitances with theoretical values (points) and the corresponding fractional coverage of the 3 dipole states: towards surface (↑), away from (↓) & parallel to ( ). The dimer of (c) has no dipole moment.

has extended his basic model to allow for solvent clusters by including an additional fitting parameter. The result for N-methyl formamide, for which only dimers with no overall dipole moment were allowed, is shown in Figure 3.4 (c)[87]. It can be seen that the theory is still relatively poor except when σ_m is large and negative which implies that a more sophisticated model is required.

All the attempts to obtain C_{dipole} mentioned above have considered the solvent as discrete particles only in the compact layer and it is still modelled as a continuum in the diffuse layer. Carnie and Chan[88], however, considered the electrolyte as a whole and modelled it as a mixture of hard spheres with embedded point charges and hard spheres with embedded point dipoles. These authors considered the structure of this model electrolyte at a charged hard wall in the MSA. No computer simulation results for this system are available as yet.

In general, modelling of highly-associated solvents is extremely difficult as is evidenced by the small amount of progress that has been made for bulk solvents despite the considerable amount of work carried out on such systems. However, it is clear from Figure 3.4 and the discussion of section 3.2 that the solvent structure near to the metal surface is an important feature of the interface making the use of a more sophisticated model essential for better agreement between theory and experiment.

The other feature which must be included in models of the compact layer is the chemistry of the physical system. Fawcett estimated the short-range chemical interactions in his model[84], but in most other attempts they are estimated indirectly through studying the extent of specific adsorption[6,54]. This latter

term refers to a situation when some of the electrolyte ions (usually anions) are in direct contact with the metal, ie. with no solvent layer between the ions and the metal. Such an interaction occurs in most systems of interest as can be seen from the dependence of properties of the compact layer on electrolyte concentration[54]. Apart from concentration, specific adsorption depends on other factors such as ion size and nature, and the sign and magnitude of σ_m .

For quantitative study of specific adsorption a more precise definition is required. It has been formally defined in several different ways, but a practical definition can be provided in terms of relative surface excesses, the latter being well-defined, observable, thermodynamic quantities. With this definition specific adsorption is said to occur if there is a surface excess (compared with the bulk) of ions with the same sign charge as that on the metal or an excess of either type of ion if the electrode is uncharged. To obtain the specifically adsorbed charge (and thus the capacitance) from the measured relative surface excesses an assumption must be made about the distribution of the non-specifically adsorbed ions. In practice this means invoking diffuse layer theory, but unfortunately, at the concentrations at which specific adsorption occurs ($\geqslant 0.1M$[54]) it is known (see section 3.2) that this theory is not a good approximation.

The use of diffuse layer theory in this way has hampered development of a proper theory for the capacitance of the compact layer. However, specific adsorption and the compact layer have been studied in considerable detail through adsorption isotherms[54,89]. These give the extent of coverage of the electrode by each species in the electrolyte. They vary widely in complexity,

a simple one being that of Langmuir[90]. Most involve interaction parameters which are generally qualitative, empirical quantities. They are usually included to obtain a fit with the experimental data although there have been some attempts to give the parameters a molecular basis. Bockris, Devanthan & Muller[91] have developed more sophisticated isotherms by including repulsions between the ions parallel to the electrode, field dipole interaction and the image interactions arising because of the sharp change in dielectric constant across the metal-electrolyte interface. They also looked at the variation of the dielectric constant, ε , of the electrolyte in the interface region. From considerations of image interactions they concluded that, for water, ε rises smoothly from ~ 6 for the first layer of water molecules to the bulk value within a distance of ~ 12Å from the electrode.

In summary, then, in the absence of specific adsorption, a good quantitative description of the compact layer is possible except for highly associated solvents, such as water, when the description is only qualitatively correct. For systems in which specific adsorption occurs emphasis has been put on theories giving the extent of this adsorption, but despite the existence of some relatively sophisicated treatments, it is still not possible to predict the capacitance. This is partly because the diffuse layer theory is poor at the concentrations found in these systems. Broadly speaking, the theories of the electrified interface predict the behaviour most successfully for systems of relatively little interest to experimentalists. The metal-aqueous electrolyte interface, of particular importance to the latter group, is poorly described because of the particularly complex nature of water as a solvent.

Chapter 4 The mean spherical approximation for molten alkali halides near a hard wall

In the last two chapters we concentrated on the metal-aqueous electrolyte interface looking both at the experimental data and the theoretical work. Several points emerge. First, the water present in the interface determines the latter's properties to a large extent. Second, the solvent structure is not included in most models of the double layer and therefore this omission is a serious weakness. Finally, the inclusion of the water structure is not easy as there is no good model for the bulk structure; some progress can be made for simple solvents.

Because of the problems associated with water, and to a lesser extent other solvents, we have decided to turn our attention to systems where molten salts are the electrolytes. For these systems there is no solvent present so that it is more reasonable to model the electrolyte using the restricted primitive model, ie. as charged hard spheres in a dielectric continuum (see section 2.2). It is rather suprising, therefore, that until now no such application of this model or a similar one appears to have been made. Indeed, there appears to be no application of any model to metal-molten salt interfaces. Here, we have used the mean spherical approximation (MSA) as a description of the molten salt electrolyte, while the electrode has been considered simply as a hard wall. In this chapter we give details of our work and the results of the calculations using the MSA. In addition, in section 4.5 the latter are compared with our results using the exponential approximation, details of which are to be found in Appendix D.

4.1 Preliminary considerations

Initially interfaces with molten salt electrolytes were considered by us because of the difficulties of modelling aqueous electrolytes. Analysis of the limited experimental data available for molten salt systems led to Figure 4.1 in which the inverse of the differential capacitance at the point of zero charge, $(C^{pzc})^{-1}$, is plotted as a function of temperature. The data are for molten alkali halides in contact with a lead electrode[92]. Note that in all cases $(C^{pzc})^{-1}$ decreases monotonically with temperature over the ranges studied. Comparison of Figure 4.1 with the corresponding curves for aqueous electrolytes (Figure 3.3) immediately reveals a qualitative difference between the two sets of curves, namely that the temperature dependence has changed sign. Closer examination of Figure 4.1 with regard to the magnitude of the capacitance shows that:

(i) the inverse capacitance increases with increasing size of cation, for a chosen anion (excluding the lithium salts);

(ii) there is an insensitivity of $(C^{pzc})^{-1}$ to changes in the anion, for a chosen cation.

Thus, any successful model of metal electrode-molten alkali halide systems should predict these three features of the experimental $(C^{pzc})^{-1}$ versus temperature curves as well as giving the correct magnitude of the capacitance. No simple model is likely to explain the anomalous position of lithium in this figure. In the aqueous chemistry of alkali halide salts lithium's behaviour is also frequently anomalous: this is a consequence of an exceptionally strong hydration of the Li^+ ion.

A starting point for a model is the Gouy-Chapman theory

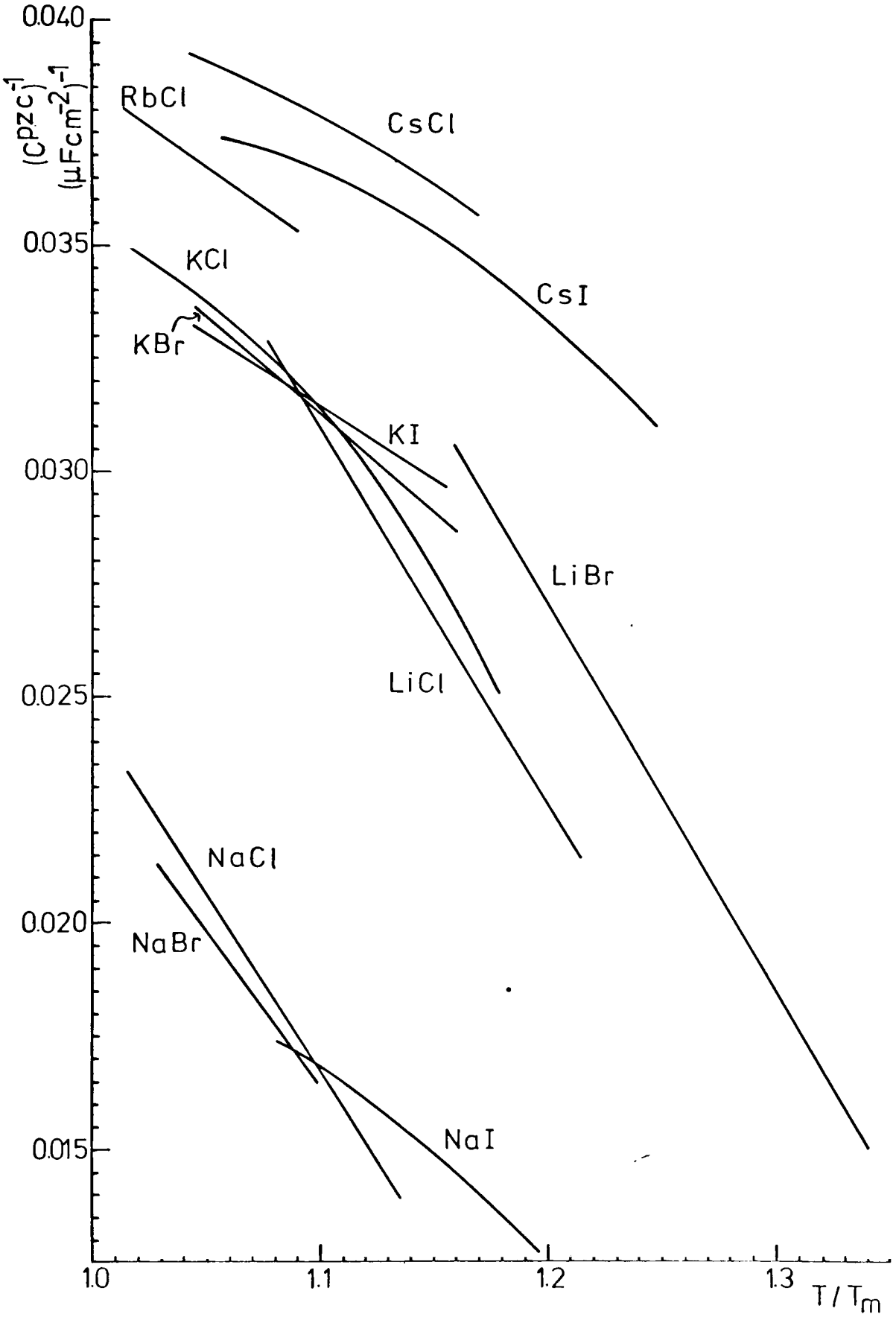


Figure 4.1 Experimental inverse capacitances at PZC for lead-molten alkali halide systems as a function of T/T_m.

(section 2.1) although at first sight it seems unlikely to be successful since it predicts a temperature dependence, viz. $C \propto T^{-1/2}$ opposite to that observed and the differences between systems with different electrolytes enters only through the dielectric constant. However, some progress can be made by considering the interpretation of n, the density of screening carriers, which occurs in the Gouy-Chapman equation for C^{PZC} (equation (3.1)). For aqueous electrolytes n is simply the density of ions in the solution, but its interpretation is not so straightforward for molten salts.

For ionic crystals just below the melting point the density of carriers available for screening the charge on the electrode is directly related to the local density of defects. This number has a Arrhenius temperature dependence. For molten salts not far above the freezing point a variety of experiments, including computer simulation and neutron diffraction, has shown that there is a strong short-range ordering present[93,94] revealing similarities in the properties of the two phases over a limited temperature range. Thus, by analogy with the solid, we may postulate the charge-ordering which gives a temperature dependence of n that opposes the explicit $T^{-1/2}$.

It is reasonable to suppose that the effect on the surface charge density profile (in an ionic crystal with Schottky defects dominant) of applying an electric field will depend on the difference between the formation energy of anion and cation vacancies, ΔE. This dependence has been suggested by the work of Eshelby et al[95] on charged dislocations in ionic crystals. It is supported by the experimental results shown in Figure 4.2 in which $d((C^{PZC})^{-1})/d(T/T_m)$, with T_m the melting temperature, is plotted against ΔE.

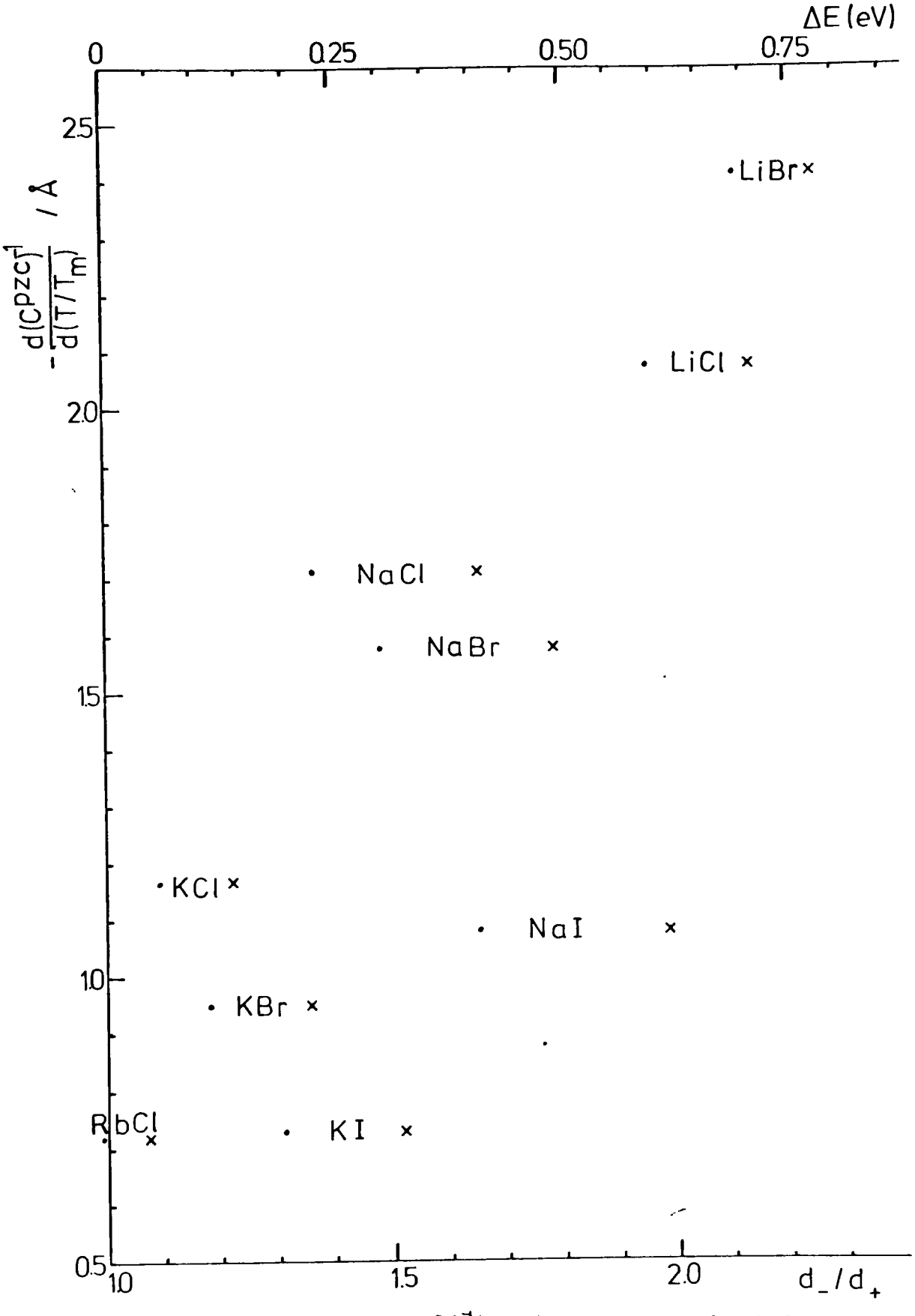


Figure 4.2 The variation of $d(C^{pzc})^{-1}/d(T/T_m)$ values derived from the curves in Figure 4.1 with the theoretical quantities ΔE (crosses) and d_-/d_+ (points).

Calculated values for ΔE were taken from Hardy and Karo[96]. A distinct correlation may be seen from the figure, which is further evidence that the crystal analogy is relevent to the molten salt data.

It is unsatisfactory to discuss molten salt structure in terms of point defects. However, the Hardy-Karo values of ΔE themselves correlate strongly to the radius ratio of anions to cations, r_-/r_+, which is an important quantity characterising molten salts. This correlation can be seen in Figure 4.2 where $d(C^{pzc})/d(T/T_m)$ has also been plotted against d_-/d_+, values of the latter for molten salts being taken from Abramo et al[97].

In summary, there is considerable evidence that, near the freezing point, molten salts are significantly charge-ordered and - drawing on theory which holds for ionic solids at similar temperatures - that this may have a dominant effect on the temperature dependence of C^{pzc}. Thus, we need to look at a model, not related to the solid, which describes the short-range ordering in molten salts.

For bulk molten salts it is known[93,94] that the mean spherical approximation gives the structural correlations between unlike ions well, but those between like ions less well, and that it reproduces the general trend of the structural features of the short-range charge ordering. Thus it seems reasonable to apply this model to the interface. The MSA has the advantage that it is sufficiently simple to yield some analytic results for interfacial systems (see section 4.3 and Appendix B). It is also worthy of note that for an uncharged electrode the MSA becomes equivalent to the Gouy-Chapman theory in the limit of the hard sphere diameters

going to zero. In this sense, therefore, it can be regarded as an extension of the latter theory.

4.2 The Ornstein-Zernike equation for a two-component system in contact with a hard wall

The departure of the pair correlation function from its perfect gas value of unity is a measure of the influence of one molecule on the distribution of another. This departure is the total correlation function, $h(r_{12})$, which for a one-component, homogeneous fluid is given by:

$$h(r_{12}) = g(r_{12}) - 1 \tag{4.1}$$

with $g(r_{12})$ being the corresponding pair correlation function and $r_{12} = |\underline{r}_1 - \underline{r}_2|$. Ornstein and Zernike[13] suggested a division of into two parts, a direct part and an indirect part. The direct part, which is the direct influence of molecule 1 on molecule 2, is defined as being the direct correlation function, $c(r_{12})$. The indirect part is the influence (on molecule 2) from molecule 1 on molecule 3. This influence on molecule 2 is exerted directly or indirectly through other molecules. The extent of this indirect part is a density-weighted average over all positions of molecule 3.

With this division of $h(r_{12})$ we may write:

$$h(r_{12}) = c(r_{12}) + n\int c(r_{13})\, h(r_{23})\, d\underline{r}_3 \tag{4.2}$$

This equation is called the Ornstein-Zernike equation. The subscripts for the correlation functions under the integral sign

may be interchanged for an isotropic liquid. Equation (4.2), which is for a one-component fluid, may be easily generalised for an n-component one:

$$h_{ij}(r_{12}) = c_{ij}(r_{12}) + \sum_{k=1}^{n} \rho_k \int c_{ik}(r_{13}) h_{kj}(r_{23}) d\underline{r}_3 \qquad (4.3)$$

The system of most interest in this work, however, is one where a two-component liquid is in contact with a wall. This can be modelled by considering a mixture of three types of particles one of which, with subscript o, is very large in size, but small in concentration[28]:

$$\begin{aligned} \rho_o &\to 0 \\ R_o &\to \infty \end{aligned} \qquad (4.4)$$

such that

$$\rho_o R_o^3 \to 0 \qquad (4.5)$$

where R_o is the hard sphere radius of the particle o. The molecules of the remaining species see the third type of species as a planar wall in the limit $R_o \to \infty$. The interaction between these 'wall particles' is essentially zero because of condition (4.5) which implies a large separation.

For this particular case the Ornstein-Zernike equation is written[28]:

$$h_{oi}(r) = c_{oi}(r) + \rho \sum_{j=1}^{2} \int c_{ij}(s) h_{oj}(\underline{r} - \underline{s}) d\underline{s} \qquad (4.6)$$

where the subscripts on r have been dropped for simplicity. ρ

is the bulk number density of the liquid. Changing to bipolar coordinates:

$$h_{oi}(r) = c_{oi}(r) + \frac{2\pi n}{r} \sum_{j=1}^{2} \int_0^\infty ds\, s\, c_{ij}(s) \int_{|r-s|}^{r+s} dt\, t\, h_{oj}(t) \tag{4.7}$$

where r is the distance from the centre of the wall particle to a particle of type i whereas the distance of interest, x, is that from the wall to the particle i. The distances r and x are related by:

$$r = R + x \tag{4.8}$$

where

$$h_{oi}(R+x) = h_{wi}(x)$$

$$c_{oi}(R+x) = c_{wi}(x) \tag{4.9}$$

the new notation emphasising the change from 'wall particle' to wall. Equation (4.7) becomes, with similarly, $t = R+u$:

$$h_{wi}(x) = c_{wi}(x) + \frac{2\pi n}{(R+x)} \sum_{j=1}^{2} \int_0^\infty ds\, s\, c_{ij}(s) \int_{x-s}^{x+s} du\,(R+u)\, h_{wj}(u) \tag{4.10}$$

and in the limit that $R \to \infty$:

$$h_{wi}(x) = c_{wi}(x) + 2\pi n \sum_{j=1}^{2} \int_0^\infty ds\, s\, c_{ij}(s) \int_{x-s}^{x+s} du\, h_{wj}(u) \tag{4.11}$$

Thus, this is the Ornstein-Zernike equation for a two-component system in contact with a hard wall.

4.3 The MSA for a mixture of ions in contact with a hard wall

Before results can be obtained from equation (4.11) certain approximations must be made since all the correlation functions contained in it are unknown. This is a problem general to integral equation approaches and it has already been discussed in section 2.3. The closure approximation used here is the mean spherical approximation in which an explicit form, in terms of the interaction potential, is given for the direct correlation functions of equation (4.11). This equation may then be solved for the radial distribution function.

The MSA was proposed by Lebowitz and Percus[35] and may be expressed by two equations, namely:

$$g_{\alpha\beta}(r) = 0 \qquad r < d_{\alpha\beta} \tag{4.12}$$

$$c_{\alpha\beta}(r) = -\beta u_{\alpha\beta}(r) \qquad r > d_{\alpha\beta} \tag{4.13}$$

Hard cores are thus an integral part of the model with $d_{\alpha\beta}$ the distance of closest approach of the centres of the hard spheres:

$$d_{\alpha\beta} = \frac{1}{2}(d_\alpha + d_\beta) \tag{4.14}$$

where d_α and d_β are the hard sphere diameters. Equation (4.13) becomes exact in the limit of large r. To solve the MSA a form for the pair potential $u_{\alpha\beta}(r)$ must be chosen.

In the present case we must consider the interaction of i- and j-particles with each other and with the wall. Here, the ionic melt is represented by the primitive model (section 2.2) so

that the interionic pair potentials are given by (cf. equation (2.31))

$$u_{ij}(r) = \infty \qquad r < d_{ij}$$
$$= \frac{z_i z_j e^2}{\varepsilon r} \qquad r > d_{ij} \tag{4.15}$$

There must be overall charge neutrality so that for two ionic species

$$\sum_{i=1}^{2} n_i z_i = 0 \tag{4.16}$$

From equation (4.13) and (4.15) the direct correlation function of the bulk molten salt is:

$$c_{ij}(r) = -\frac{\beta z_i z_j e^2}{\varepsilon r} \qquad r > d_{ij} \tag{4.17}$$

The pair potential between the hard wall and the charged hard spheres of the electrolyte is also given by a hard core repulsion and a coulombic tail. Since the wall is planar, the latter has a different form[98]:

$$u_{wi}(x) = -\frac{4\pi \sigma_m z_i e x}{\varepsilon} \qquad . \; x > d_i/2 \tag{4.18}$$

with the wall at $x=0$. σ_m is the charge per unit area on the wall. Equation (4.18) leads to:

$$c_{wi}(x) = \frac{4\pi\beta \sigma_m z_i e}{\varepsilon} x \qquad x > d_i/2 \tag{4.19}$$

The solution of equation (4.11) with (4.17) and (4.19) is effected by the Baxter technique[99], an outline of which can be

found in Appendix A. The pair correlation function between the wall and the ions, $g_{wj}(x)$, in the MSA is given by[98]:

$$g_{wj}(x) - \sum_{l=1}^{2} n_l \int_{\lambda_{jl}}^{x-d_l/2} dr\, g_{wl}(x-r) Q_{lj}(r) = \frac{1}{2\pi} Q_j'' - F_j(x) \qquad x > d_j/2 \tag{4.20}$$

using the notation of Appendix A. $F_j(x)$ is a quantity which vanishes at the point of zero charge so that near a neutral hard wall $g_{wj}^{PZC}(x)$ is:

$$g_{wj}^{PZC}(x) - \sum_{l=1}^{2} n_l \int_{\lambda_{jl}}^{x-d_l/2} dr\, g_{wl}(x-r) Q_{lj}(r) = \frac{1}{2\pi} Q_j'' \qquad x > d_j/2 \tag{4.21}$$

The value of $g_{wj}^{PZC}(x)$ at $d_j/2$ is, from equation (4.21):

$$g_{wj}^{PZC}(d_j/2) = Q_j''/2\pi \tag{4.22}$$

while for $x < d_j/2$ it is of course zero.

The differential capacitance of the hard wall-MSA system, C_{MSA}, may be fairly readily obtained as follows. The potential drop, $\Delta\psi$, across the interface, ie. the difference in potentials at the surface of particle ω and infinity, can be derived from the Poisson equation and the definition of $g_{wj}(x)$:

$$\Delta\psi = -\frac{4\pi e}{\varepsilon} \int_0^\infty dx\, x \sum_j \rho_{wj}(x) = \frac{4\pi e n}{\varepsilon} \lim_{s\to 0} \left[\frac{d}{ds} \tilde{g}_{wj}(s) \right] \tag{4.23}$$

where $\tilde{g}_{wj}(s)$ is the Laplace transform of $g_{wj}(x)$. The capacitance is then obtained in terms of σ_m and $\tilde{g}_{wj}(s)$ through equation (1.8):

$$\frac{1}{C_{MSA}} = \frac{4\pi e n}{\varepsilon} \frac{\partial}{\partial \sigma_m} \left\{ \lim_{s\to 0} \left[\frac{d}{ds} \tilde{g}_{wj}(s) \right] \right\} \tag{4.24}$$

At the point of zero charge this becomes:

$$\frac{1}{C^{pzc}_{MSA}} \simeq \frac{4\pi e n}{\varepsilon} \frac{\partial}{\partial \sigma_m} \left\{ \lim_{s \to 0} \left[\frac{d}{ds} \tilde{g}^{pzc}_{ij}(s) \right] \right\} \qquad (4.25)$$

Equation (4.25) is a quite general equation, which will usually have to be evaluated numerically. In the case of the MSA, however, Blum[100] has shown that, for equal diameter ions, an analytic form of C^{pzc}_{msa} may be obtained:

$$C^{pzc}_{msa} = \frac{\varepsilon}{4\pi} \cdot 2\Gamma \qquad (4.26)$$

where the parameter 2Γ is a generalisation of the Debye-Huckel screening length, K_D, and for equal ionic diameters is given by:

$$\Gamma d = \frac{1}{2} \left[-1 + (1 + 2K_D d)^{\frac{1}{2}} \right] \qquad (4.27)$$

with $K_D = (8\pi n e^2 / \varepsilon kT)^{\frac{1}{2}}$ and $d_+ = d_- = d$. For ions of different sizes the complexity of the equations involved in Blum's approach becomes considerably greater and the capacitance of such a system has not yet been obtained by this method. However, by taking a more physical approach we have been able to obtain an expression for the more general system. The details are given in Appendix B. The result may still be written in the form of equation (4.26), taking the general form of Γ given in Appendix A. Our result shows that the capacitance predicted using the MSA is independent of the charge on the electrode. However from the appearance of the experimental curves[92] this is a weak feature of the model.

It is possible, in principle, to split C_{msa} into a compact

layer part and a diffuse layer part in order to make contact with GCS theory. However, when this is done, as we show in Appendix C, the diffuse layer part has an unphysical temperature dependence. Thus, the MSA theory differs from this earlier theory at a very fundamental level.

In contrast, Gouy-Chapman theory can be recovered from the MSA theory in the limit of low ionic concentration in which equation (4.27) becomes:

$$2\Gamma = K_D \tag{4.28}$$

and equation (4.26) becomes identical with the corresponding Gouy-Chapman expression (3.1). The MSA represents an improvement on Gouy-Chapman theory because ion size is taken into account; as discussed in section 2.2 ion size effects will always be negligible in the low concentration limit. In molten salt systems this limit is never realised.

To use the expression (4.26) we need the effective dielectric constant, ε . Few data for ε for molten salts are available, although estimates are available for LiCl and NaCl from refractive index measurements[101]. These experimental values are in good agreement with theoretical values for the crystalline forms obtained from the electronic polarisabilities, α_i , of the ions, using the Clausius-Mossotti relationship[102]:

$$\frac{M}{n}\,\frac{\varepsilon-1}{\varepsilon+2} = \frac{4\pi}{3}\sum_i n_i\alpha_i \tag{4.29}$$

Here, M is the molecular weight; n , the bulk density; and n_i ,

the number density of ions of type i . Values of ε were calculated using (4.29) with temperature-dependent molten salt densities obtained from Janz[101]. The remaining parameters required to calculate C^{PZC} from (4.26) are the ionic diameters, d_+, d_- . These, including their weak temperature dependence, are taken from the work of Abramo et al[97].

4.4 Numerical results for the MSA

The main results for the hard wall-molten salt interface using the MSA are shown in Figures 4.3-4.6. We shall consider each figure in turn.

In Figure 4.3 the inverse values of the calculated differential capacitance for molten alkali halides are plotted as a function of temperature. This figure may be directly compared with Figure 4.1, the corresponding experimental curves for the lead-molten alkali halide systems. From these two figures it can be seen that the magnitude of the calculated capacitance is in approximate agreement with the experimental values. In addition the appreciable dependence of the measured capacitance on the cation for fixed anion and the insensitivity to changing the anion for fixed cation are qualitatively reproduced by the model.

As anticipated the anomalous position of the lithium salts is not explained; this suggests that some aspect of the lithium salt melt is absent from the model we have developed.

The temperature dependence of $(C^{PZC}_{MSA})^{-1}$ is appreciably weakened from the Gouy-Chapman prediction of $T^{1/2}$ although it is still in qualitative disagreement with the experimentally observed

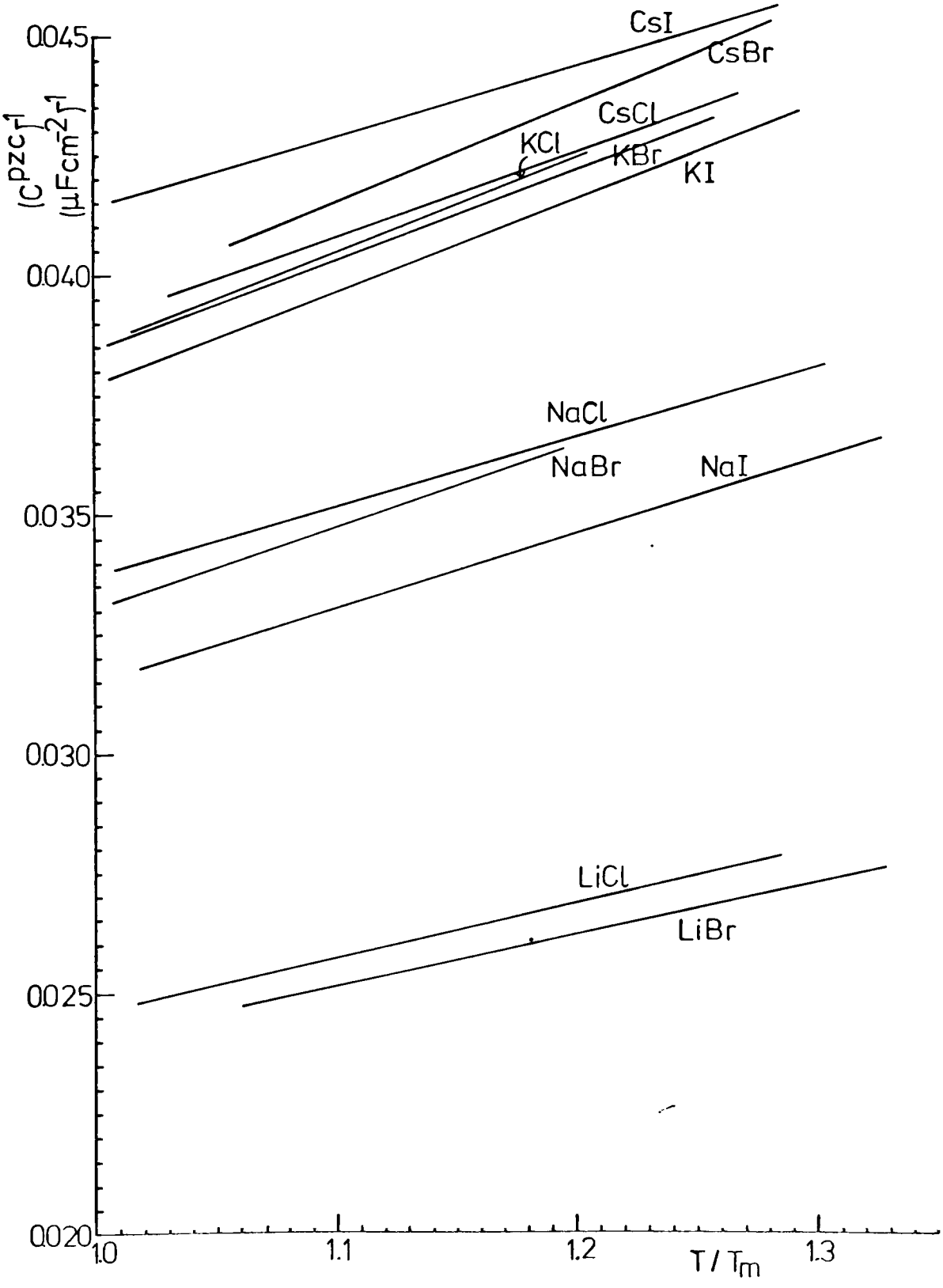


Figure 4.3 Inverse capacitance values calculated in the MCA from equation (4.26) as a function of T/T_m .

trend. Thus, it can be concluded that the hard wall-MSA model is relatively successful in predicting the experimental curves of Figure 4.1 although the sign of the temperature dependence is still incorrect. It is certainly significantly more successful than similar models are when applied to systems involving aqueous electrolytes. The likely reasons for this are now discussed.

Any solvent capable of dissolving an ionic crystal to an appreciable extent has to have a high dielectric constant, one which is much higher than that of the electrode. From theoretical considerations the dielectric constants of metals are thought to be the order of 1[103] and recently Ford and Weber[104] have estimated that ε for mercury is 2. However, for aqueous electrolytes the bulk dielectric constant is about that of water ($\sim$80) and the lowest estimates in the interface region are $\sim$ 6[54]. Such a disparity of dielectric constant creates image forces which are difficult to model and are ignored in most theories including Gouy-Chapman theory and the present one. In contrast, the values of the dielectric constants for molten alkali halides calculated here using equation (4.29) lie between 1 and 2. They are thus very similar to that of the metal and therefore the assumption of a single dielectric constant holds well for such systems. The success of the present, fairly simple, model suggests that the quantitative failures of more complex models of aqueous and other solvent systems is largely a consequence of their failure to take account of these solvent effects.

In molten salt systems we can therefore safely ignore the effects arising from a difference between the dielectric constants of electrode and electrolyte. It is still necessary, however, to

include the effects of polarisation of the electrolyte by using realistic values for the magnitude of this (common) dielectric constant if accurate estimates of C^{PZC} are to be obtained from equation (4.26). For example, for KCl at 800°C a value of ε =1.78 (calculated from (4.29)) gives C^{PZC} as 25.6 μFcm^{-2} whereas a value of ε =1.00, which ignores polarisation, gives a value of 17.0 μFcm^{-2}. This latter value is in much poorer agreement with the experimental value of 28.8 μFcm^{-2} than the former.

The wall-ion pair distribution functions for LiBr and KCl at two temperatures are shown in Figures 4.4 and 4.5. The cation and anion distribution show the same qualitative behaviour with, as expected, a loss of structure in the liquid as the temperature is raised. The two examples given have extreme radius ratios. For KCl, for which the ions have very similar sizes, the peaks of $g_{w+}(r)$ and $g_{w-}(r)$ occur at similar distances from the wall, while for LiBr the peaks of one distribution function approximately coincide with the troughs of the other.

The potential difference, $\Delta\psi^{PZC}_{MSA}$, between the uncharged hard wall and the model molten salt is related to the ionic distribution function by equation (4.23) in the limit $\sigma_M \to 0$ (when $g_{wi}(x) \to g^{PZC}_{wi}(x)$). It is clear from this equation that $\Delta\psi^{PZC}_{MSA}$ would be zero for equal ionic radii and that it represents the separation of the ionic charge due to the difference in size of the two species in contact with the wall. The values of $\Delta\psi^{PZC}_{MSA}$ calculated for the molten alkali halides are shown in Figure 4.6. The sign of $\Delta\psi^{PZC}_{MSA}$ and its appreciable dependence on the cation are consistent with a picture in which the smaller cations approach more closely than the anions to the wall. This was also seen in

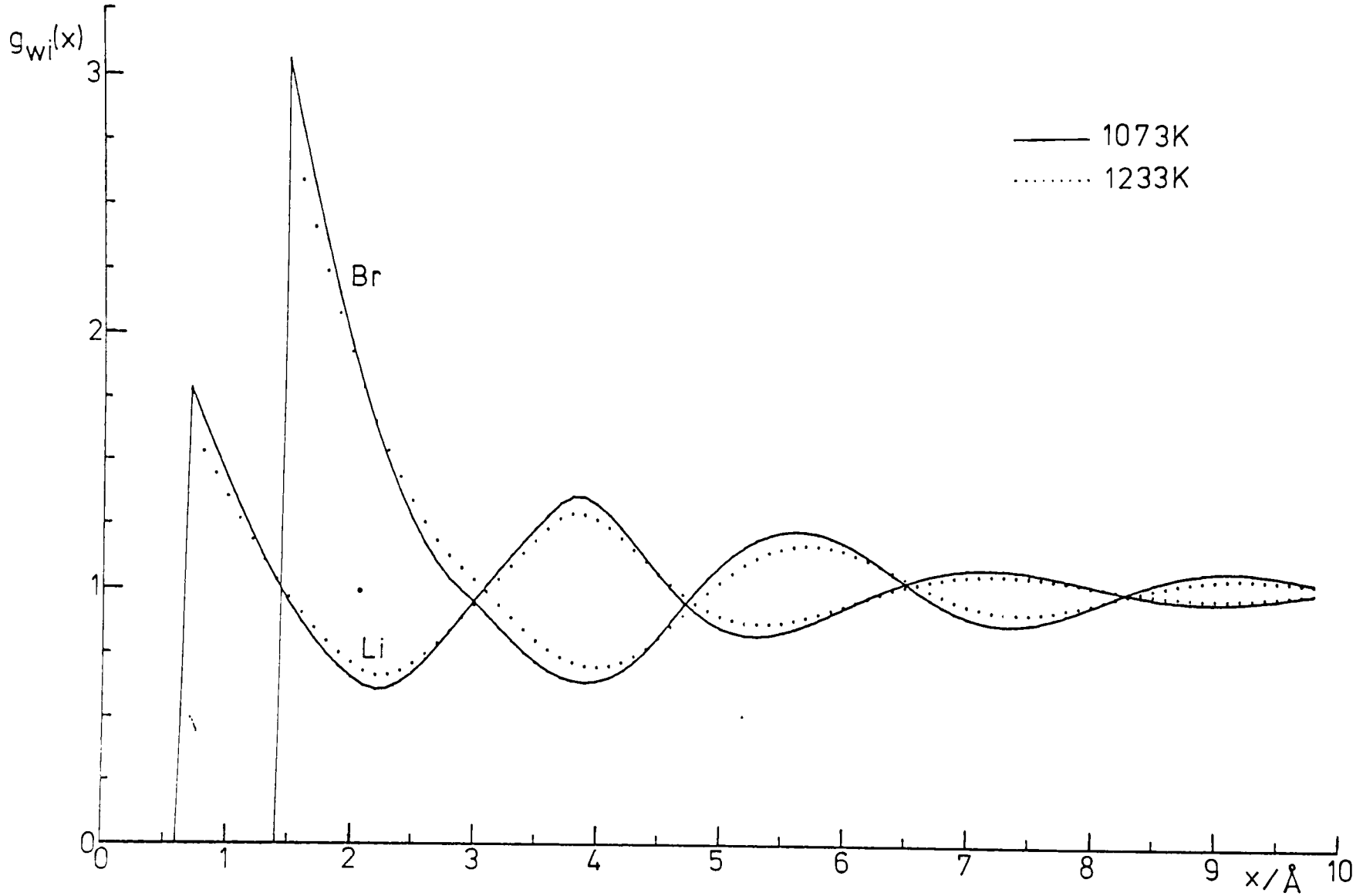


Figure 4.4 MSA wall-ion distribution functions for molten LiBr at two temperatures.

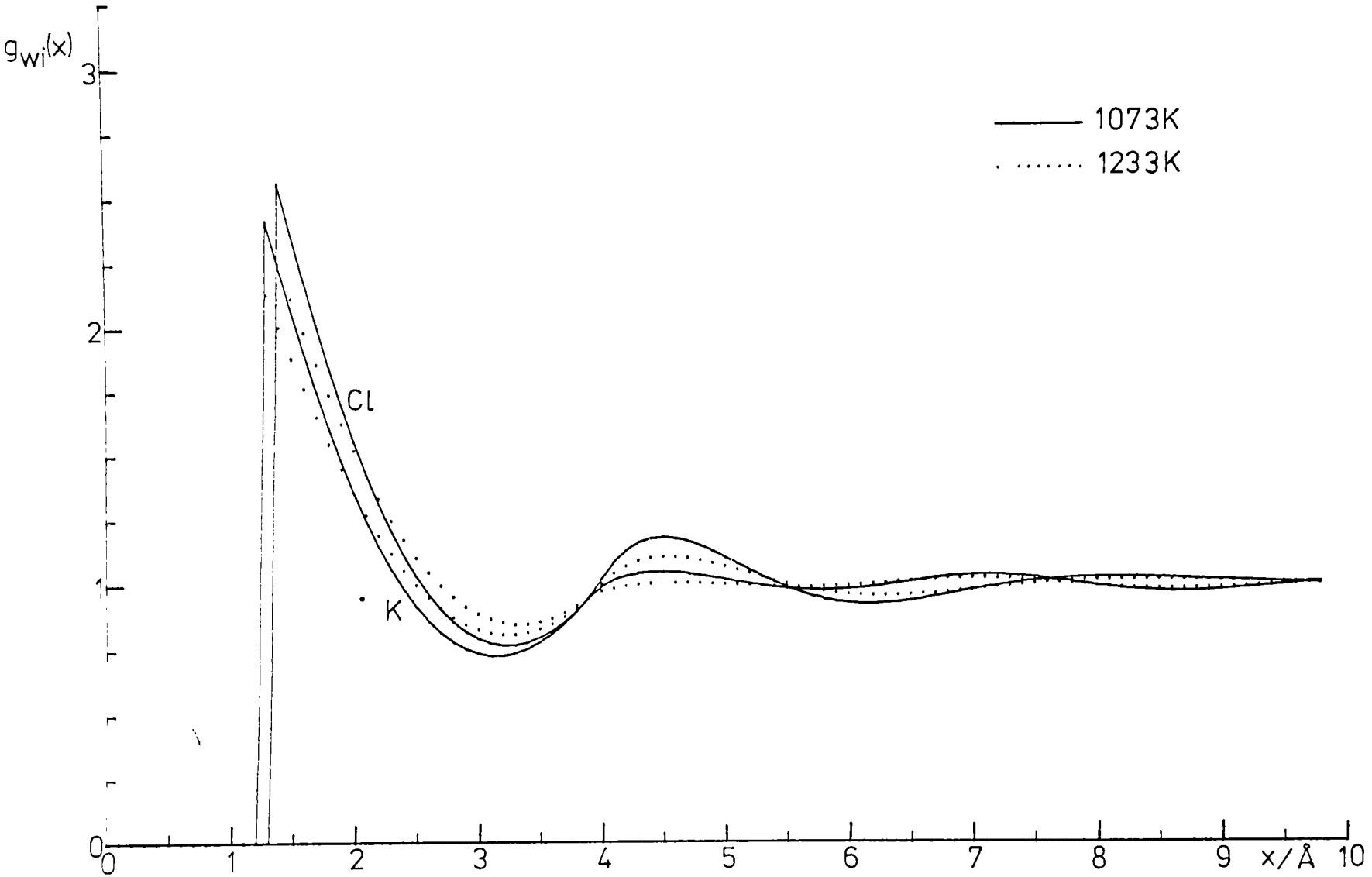


Figure 4.5 MSA wall-ion distribution functions for molten KCl at two temperatures.

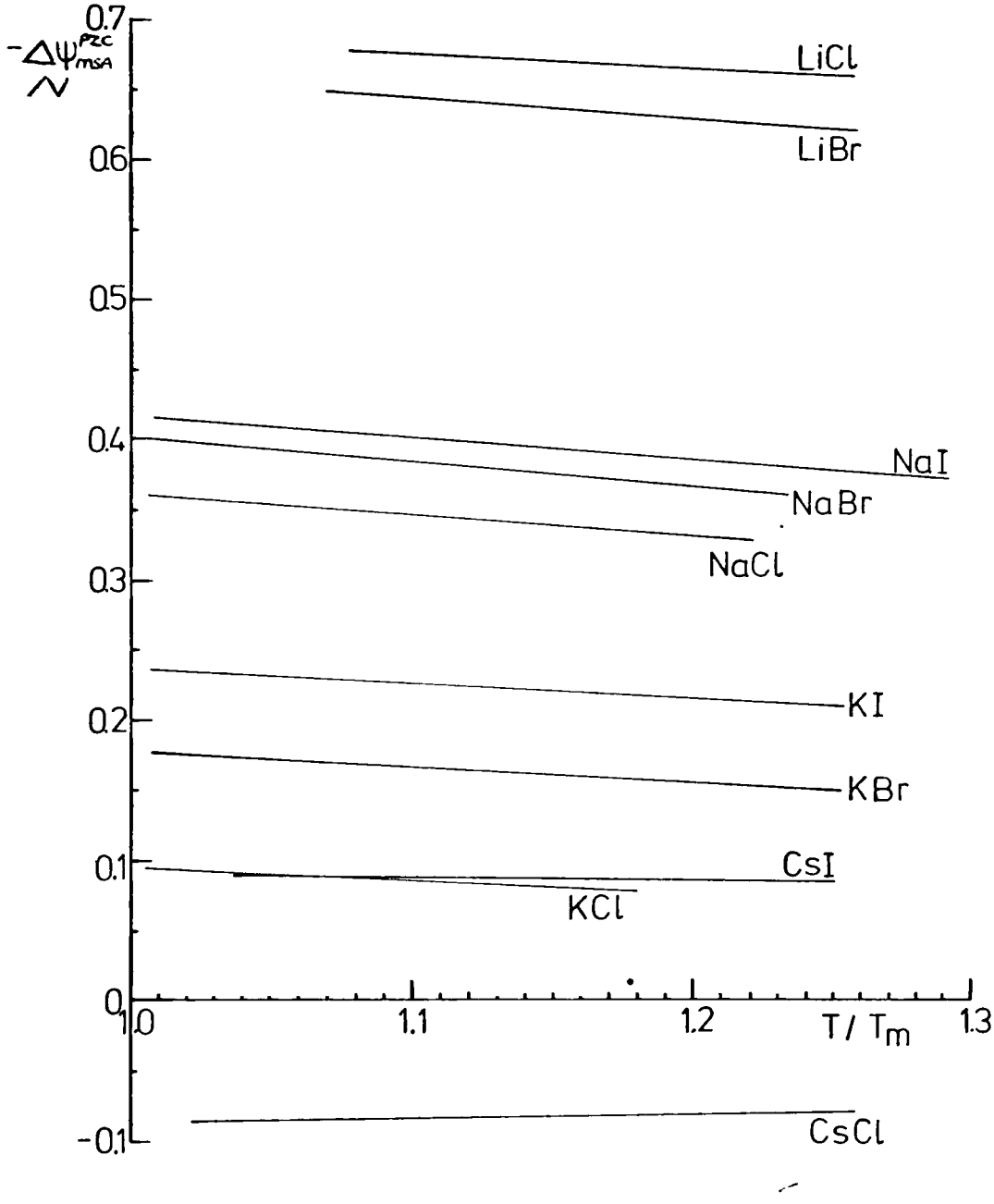


Figure 4.6 The potential difference between the hard wall and the model (MSA) molten salt.

Figures 4.4 and 4.5. There is only one exception to this in the cases considered, namely CsCl. For this salt the anion is smaller than the cation and the sign of $\Delta\psi^{pzc}_{MSA}$ is changed correspondingly.

Experimental values for $\Delta\psi^{pzc}_{MSA}$ cannot be compared directly with theoretical ones because they invariably involve a potential drop at a reference electrode whose value can never be measured in isolation. If the reference electrode remains unchanged, however, a comparison is possible and, up to the constant difference which we expect, there is good agreement between theory and experiment for this model[105,106]. In particular, for molten alkali chlorides [107], the dependence on the cation and the temperature dependence of the measured potential difference are given correctly by the hard wall-MSA model. From their data experimentalists[105,106] have concluded that the cations approach closer to the hard wall, in agreement with the ionic density profiles of the present model.

4.5 Beyond the MSA

The conclusion which may be drawn from the preceeding section is that the MSA successfully predicts several properties of interfaces involving molten alkali halides. Its application to these systems is quantitatively much more successful than when applied to systems involving aqueous electrolytes[37]. Nevertheless, there are still at least two features of the approximation which are unsatisfactory. These are the sign of the temperature dependence of the capacitance and the latter's independence of the charge on the electrode. Thus, improvement on the MSA is necessary if all the features of the observed differential capacitance curves for molten alkali halides are to be predicted.

As a start to finding a model of the metal-molten salt interface which is closer to the physical system than the MSA we subsequently chose to use the exponential (EXP) approximation[36] in the description of the electrolyte while still including the electrode as a hard wall. The exponential approximation was chosen because, like the MSA, it is relatively simple and because it gives better results than the MSA for bulk molten salts[93]. Much weight should not be given to the results for the bulk since, as has been seen for aqueous electrolytes[37], success in describing the bulk is no guarantee of success in describing the interface region. Blum[100] has suggested that the EXP approximation should be 'more reliable' than the MSA for interfacial systems.

The details of our calculations using the EXP approximation are given in Appendix D, but a few points of particular interest will be mentioned here briefly. The results obtained are very different to those of the MSA. Notably the sign of the temperature dependence of C_{EXP}^{pzc} is in agreement with experiment and thus opposite to that predicted by the MSA. However, on balance the EXP approximation is less successful than the MSA. The main reason for this opinion is that the capacitances obtained from the EXP calculations are far smaller than either the measured or MSA values. For instance, for KCl at 800°C the experimental capacitance is 28.8 μFcm^{-2} and that calculated using the MSA is 25.6 μFcm^{-2}. The corresponding value for the EXP approximation is 3.1μFcm^{-2}. The capacitance depends on an integration over the density profiles (this can be clearly seen from equation (D10)). Such a disparity between theoretical and experimental values for the capacitance implies that the predictions for the density profiles are seriously wrong. Investigation of equation (D10) indicated that a major cause

of this disparity is that the EXP contact values, $g_{wi}^{PZC}(d_i/2)$, are much larger than those of the MSA.

Although it is clear that the EXP approximation describes the structure of molten alkali halides near a hard wall less well than the MSA, the calculations have contributed to our understanding of the interfacial region. In particular, investigation of the density profiles revealed that the main contribution to the capacitance in both the mean spherical and exponential approximations comes from the ions in contact with the hard wall. This is discussed at more length in Appendix D.

So far in this section we have discussed an alternative reseprentation of the electrolyte which we hoped would have been an improvement on the MSA. A number of other approximations can also be applied, although generally the calculations are more involved. A particularly promising approximation is the hypernetted-chain closure of the Ornstein-Zernike equation. There is agreement between this approximation and the contact theory of Henderson et al[37] at the hard wall and the former is generally accepted to give the bulk molten salt structure most accurately[93,94]. However, success for the bulk structure may not be significant in the light of our calculations. The main disadvantage of the HNC approach is its relative complexity and the results of its application to the present system of interest are still awaited[108].

Apart from using a more realistic model of the molten salt improvement of the results from our MSA calculations may be made by considering the metal electrode in a less crude way than as a hard wall. We turn to this aspect of the interface in the next chapter and in section 5.3 show that by including some structure in the

model of the metal the results of this present chapter may be improved.

Chapter 5 The role of the metal

Up to this point the electrode has been represented as a charged, hard, planar wall often having the same dielectric constant as the bulk electrolyte. In this chapter we shall attempt to indicate some of the ways in which a real electrode surface might differ from such an idealised model.

An experimental indication of the weakness of the hard wall model of the electrode may be obtained by comparing systems which differ only in the material of the electrode. In practice this is very difficult to do. As explained in Chapter 3 most experimentally studied systems have an aqueous electrolyte so limiting the temperature range of the experiments. Also, because of severe experimental difficulties, until recently it has been impossible to make reproducible measurements on systems with solid electrodes. The combination of these restrictions means that nearly all experimental data has been collected for systems containing the dropping mercury electrode.

Most theoretical studies of the interface contain the hard wall model of the electrode because of the lack of a theory which is capable of predicting the chemical effects of the metal on the properties of the metal-electrolyte interface. Nearly all theoretical work on metal surfaces up to now has been confined to explaining their physical properties[109]. Nevertheless, some conclusions can still be drawn about the role of the metal in the metal-electrolyte interface by modelling the electrode using such models developed for free metal surfaces. The model used most usually is the jellium model since this is relatively simple (see section 5.1).

It is not obvious that the important features of the free surface, in particular the spill-out of electrons, are found when the metal is in contact with an electrolyte. In section 5.2 we discuss the results obtained when the effects of electron spill-out are incorporated into models of the interface. For systems where there is little specific adsorption the agreement with experiments is significantly improved compared with hard wall models.

In the discussion in Chapter 4 of our results from the MSA calculations for the hard wall-molten alkali halide systems, we noted that although the predictions for the temperature dependence of the capacitance were an improvement on the Gouy-Chapman model, agreement with experiment was far from perfect. In section 5.3 we introduce a parameter, which is identified as a measure of the extent of electron spill-out into the electrolyte, into the model we developed in Chapter 4. We use the parameter to fit the predicted capacitances to the observed ones. The required values of the parameter give reasonable estimates for the spill-out.

5.1 The jellium model for the free metal surface

In the jellium model an interacting electron gas, representing the valence electrons of the metal, is embedded in a uniform, continuous, positively charged background representing the positive 'ion cores'[109]. The surface is introduced by terminating the positive background abruptly; the electron gas will spill-out from this surface by virtue of its kinetic energy. This produces a stable charge separation which will be referred to here as the surface dipole to distinguish it from any additional charge, ie σ_m, which may be on the metal surface. (In papers on the free surface

this dipole is often called a double layer but we will not use this term as it may lead to confusion with the charge separation arising due to the presence of an electrolyte). Here we are interested in surface properties, but to obtain these in terms of observable ones, in particular the work function, Φ , we must also consider the bulk.

We start by considering the work done when a charged particle of species i at a point B in the bulk of a conducting material, α , is transferred to the point A in the vacuum, an infinite distance from the surface of α . This work is termed the electrochemical potential, $\bar{\mu}_i^{\alpha}$, and it depends on the nature of i because at B there are specific short-range interactions with other particles. The method of calculating $\bar{\mu}_i^{\alpha}$ suggested by Lange[110] as presented by Parsons[111] will be used here.

For convenience, α is taken to be a sphere of unit diameter. $\bar{\mu}_i^{\alpha}$ can be calculated from a combination of two models which are shown in Figure 5.1 together with the system that we started with. A separation has been made between the interactions in the bulk of α and those in the surface. The work done when particle i is transferred from B' to A' is W' and W" when it is taken from B" to A". Thus:

$$\bar{\mu}_i^{\alpha} = W' + W'' \qquad (5.1)$$

W' is generally known as the chemical potential, μ_i^{α} , of i. This is a rather misleading term since it does include electrostatic contributions when i is a charged particle. In addition polarisation interactions, dispersion interactions, etc contribute

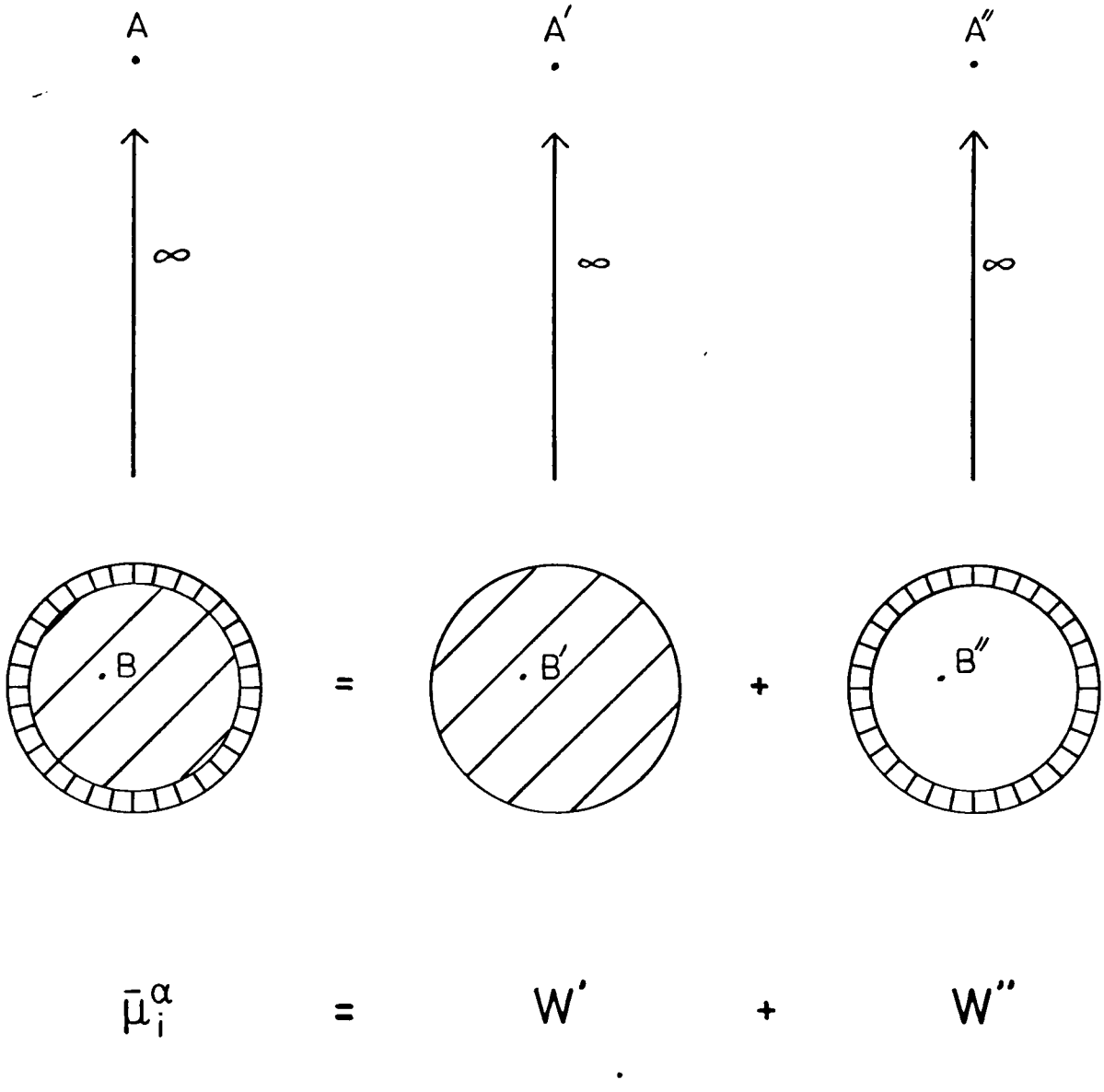


Figure 5.1 The system of interest (left) may be considered as the combination of a sphere with only bulk properties and a hollow shell.

to μ_i^α . W" arises from electrostatic interactions alone so long as B" is far enough from the shell to allow the short-range interactions between the two to be neglected. Then W" is given by:

$$W'' = z_i e \phi^\alpha \tag{5.2}$$

where $z_i e$ is the charge on particle i . ϕ^α is the potential difference between B" and A" and is known as the inner potential of α. When the spherical shell is charged there are two contributions to ϕ^α: ψ^α , the 'outer potential' of α , which is due to the free charge ($\sigma_m \neq 0$) and χ^α which is due to the surface dipole already referred to.

Thus, the electrochemical potential between A and B is:

$$\begin{aligned} \bar{\mu}_i^\alpha &= \mu_i^\alpha + z_i e \phi^\alpha \\ &= \mu_i^\alpha + z_i e (\psi^\alpha + \chi^\alpha) \end{aligned} \tag{5.3}$$

Both $\bar{\mu}_i^\alpha$ and ψ^α are experimentally observable[111] while χ^α and μ_i^α are not, so another potential, α_i^α , has been defined:

$$\alpha_i^\alpha = \mu_i^\alpha + z_i e \chi^\alpha \tag{5.4}$$

The work function, Φ , of an uncharged metal may be simply written in terms of this latter potential since when the particle transferred is an electron:

$$\Phi = -\bar{\mu}_e^m = -\alpha_e^m \tag{5.5}$$

The non-observable quantities, χ^m and μ_e^m, may be estimated using the jellium model. The electron spill-out (which gives rise to χ^m) has been calculated by Lang and Kahn[112,113] for several vlaues of bulk electron gas density, n_e, and we show in Figure 5.2 the results for two densities ($r_s=2$, $r_s=6$; $\frac{4\pi}{3}(r_s)^3 = 1/n_e$). The spill-out extends 0.1-0.2 nm which is in agreement with other calculations[114].

The values of the work function calculated using the jellium model are in reasonable agreement with the measured ones[113]. Some of the discrepancy between the theoretical and experimental values is accounted for by the over-high surface potentials, χ^m, given by this model. This results because the background positive charge is cut-off discontinuously (Figure 5.3 (a)). However, in crystalline metals the positive charge distribution is not uniform, but is made up from discrete ion cores. At the surface this corresponds to a perturbation of the jellium surface, the extent of the perturbation depending on the lattice structure at the surface. Relative to the jellium model its effect is to cause a lateral flow of electrons from high to low ionic density regions. The extreme case when there is an abrupt change in this density perpendicular to the surface is shown in Figure 5.3 (b). For actual metal surfaces the surface dipole will be determined by the balance between the opposing effects of the electron kinetic energy and the ion core lattice and in most cases χ^m will be smaller than that predicted using the jellium model.

The effect of the ion cores on the surface electronic density can be investigated by measuring the work functions of single metal crystal faces. From the above discussion, the spill-out is expected

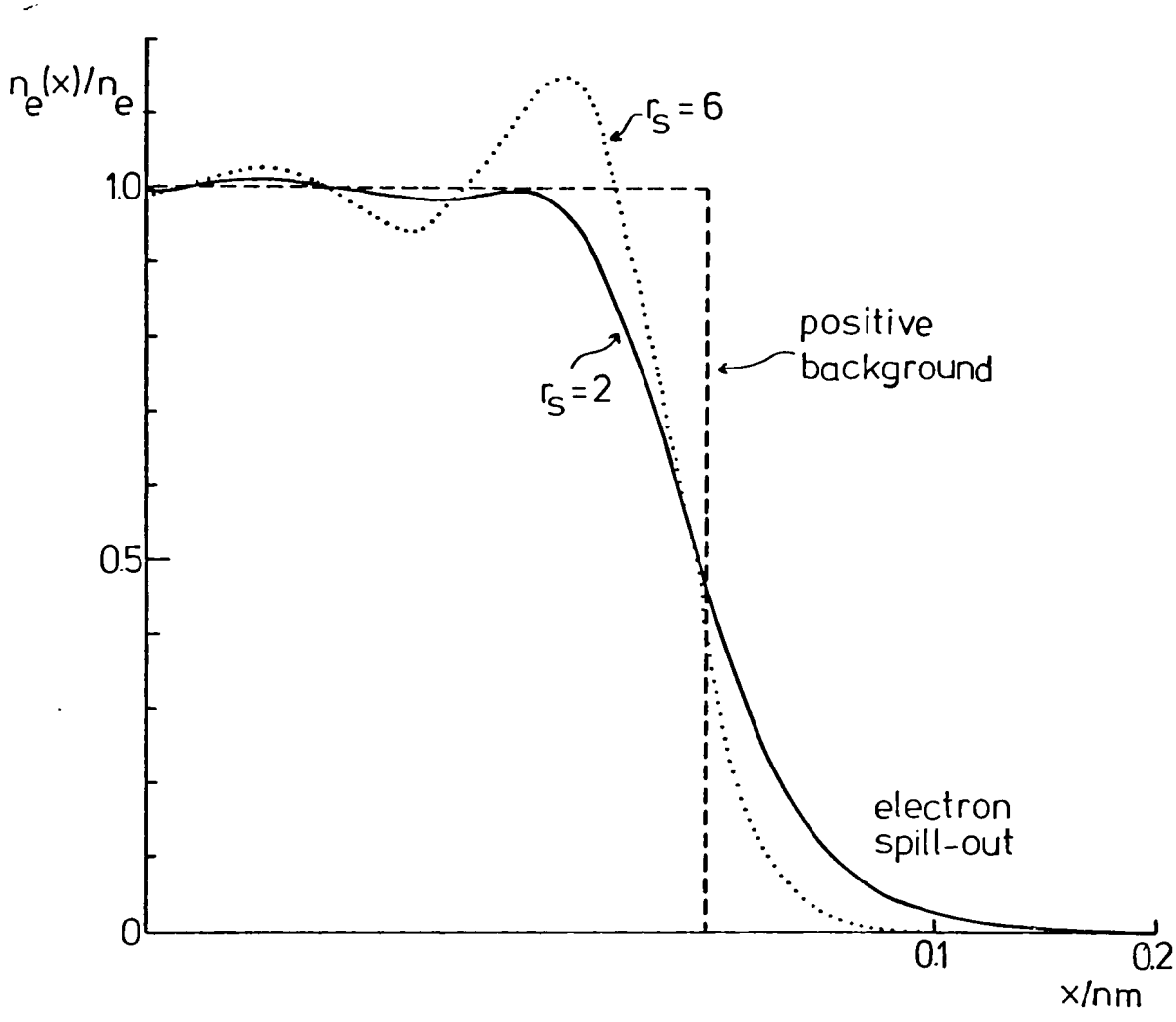


Figure 5.2 The electron spill-out calculated using the jellium model for two values of bulk electron gas density.

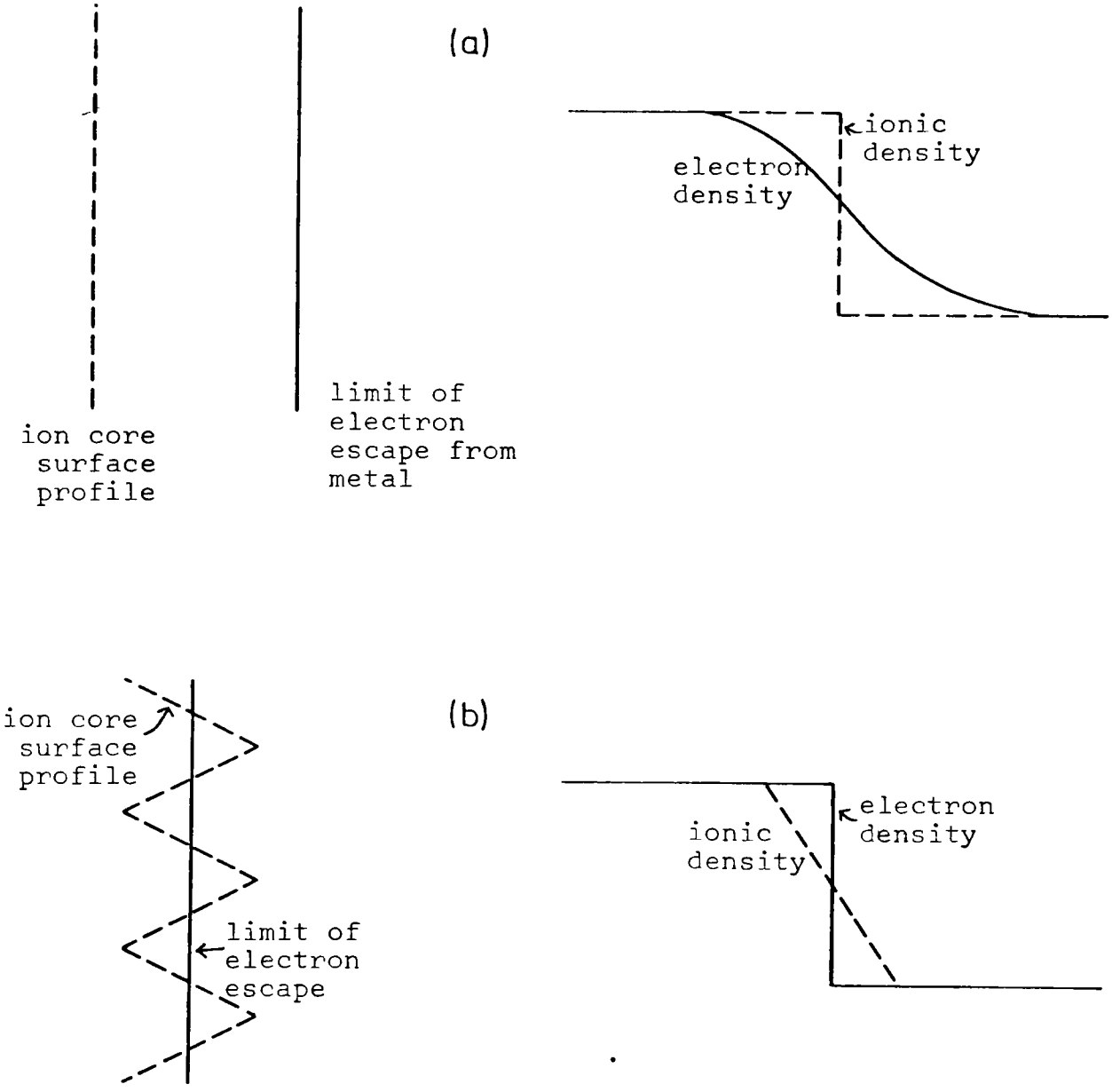


Figure 5.3 Bird's eye and side views of the metal surface for (a) the jellium model and (b) an extreme perturbation of the jellium surface due to discrete ion cores.

to be reduced, with a corresponding increase in the work function, as the surface ionic density is increased. This is exactly the trend seen[115,116]. Inclusion of a model of the ion core lattice into the jellium model has resulted in improved agreement between experimental work functions and calculated values. The average of these calculated values is typically within 8% of the observed values for simple metals, which is rather more accurate than the jellium model results (which are typically within 16%)[113].

5.2 Electron spill-out at the metal-electrolyte interface

There is general agreement that the free metal surface may be represented as a lattice of ion cores with valence electrons spilling out beyond the lattice. However, at a quantitative level there is disagreement as to the extent of the spill-out and much theoretical work still needs to be done on free surfaces. When the vacuum is replaced by an electrolyte the picture becomes even less clear. Most workers studying the metal-electrolyte interface have ignored the nature of the metal and have considered the electrode as a structureless charged hard wall. There are a few cases where the metal has been considered in more detail and in these free-surface models based on the jellium model have been used[103].

Free-surface models are only realistic when electrostatic forces are dominant so that discussion must be restricted to systems where the electrolyte is dilute and there is no specific adsorption. However, it is not clear that it is appropriate to use such models even for these systems since the 'free' electrons outside the metal surface, viewed as a chemical species, have a very high reactivity and are capable of reducing most of the solvents

commonly used for electrolytes[114]. On the other hand, a solvent for an ionic material will have a high dielectric constant which will reduce the electrostatic interaction between a solvated electron and the positively charged ionic lattice from which it has come. However, as we shall see, the use of models including electron spill-out leads to significantly better agreement with observed quantities (in particular, differential capacitance and potential at the PZC) compared with the use of models where the metal is represented as a hard wall.

In most models of the metal-electrolyte interface, including that of Gouy, Chapman and Stern, the metal is considered as a perfect conductor so that its electrostatic potential is constant. This region then makes no contribution to the capacitance of the interface. However, as we have demonstrated in the above chapters there is generally poor agreement between the measured capacitance and that predicted by such a model. It is clear that there may be a contribution to the total capacitance from the metal in which case equation (2.18) should be written as:

$$\frac{1}{C} = \frac{1}{C_m} + \frac{1}{C_c} + \frac{1}{C_d}. \qquad (5.6)$$

where C_m is this contribution. Note that equation (5.6) implies that the contribution from the metal can be completely separated from the influence of the electrolyte, ie. that the interface between the metal and the electrolyte is sharp.

One significant characteristic of C_m is that it can be expected to be independent of electrolyte concentration. For dilute electrolytes C_c is also concentration independent and the con-

centration dependence of the experimental capacitance is given well by Gouy-Chapman theory (see section 3.2). It is convenient therefore to separate these two types of contribution:

$$\frac{1}{C} = \frac{1}{C_*} + \frac{1}{C_d} \tag{5.7}$$

where C_* is concentration independent.

The magnitude of the metal capacitance will depend on the extent to which the surface potential, χ_m, differs from the bulk potential. The first attempt to quantify the contribution was made in 1928 by Rice[117]. Using the free-electron model for the metal he obtained:

$$\frac{1}{4\pi C_m} = \frac{1}{K_{TF}\sqrt{\varepsilon_b}} \tag{5.8}$$

where K_{TF} is the inverse Thomas-Fermi screening length of the free-electron gas and ε_b is the background dielectric constant of the ion cores. Values of $1/4\pi C_*$ and calculated Thomas-Fermi screening lengths are given in Table 5.1 for various simple metals. Recently, Ford and Weber[104] estimated that ε_b for mercury is 2 and for other simple metals theoretical estimates for ε_b are close to unity. For mercury, this gives $1/4\pi C_m$ =0.345Å compared with the experimental value of $1/4\pi C_*$ of 0.3Å. The results of Rice are certainly of interest, but it can be seen from Table 5.1 that, using reasonable values for ε_b, the predicted values of $1/C_*$ are rather larger than the experimental ones. Even when the values are close enough for errors and uncertainties (such as in the value of ε_b) to account for the discrepancies, these estimates allow for no concentration independent contribution from

Metal	$1/4\pi C_*$ /Å experimental	K_{TF}^{-1}/Å ($\varepsilon_b = 1$)	$(\sqrt{2}K_{TF})^{-1}$/Å ($\varepsilon_b = 2$)
Sb	0.37	0.496	0.351
Bi	0.34	0.508	0.359
Hg	0.30	0.488	0.345
Pb	0.27	0.510	0.361
Sn	0.23	0.505	0.357
Cd	0.17	0.546	0.386
In	0.11	0.526	0.372
Ga	0.07	0.502	0.355

Table 5.1: Experimental[118] and calculated (from equation (5.8)) values for the inverse capacitance, $1/4\pi C_*$; K_{TF}^{-1} was calculated from reference (119).

the compact layer. Given the weight of evidence for the existence of a compact layer for aqueous electrolytes, this suggests that the jellium model significantly overestimates the contribution from electron spill-out.

One of the few recent papers to propose any sort of model in which electron spill-out into the electrolyte is included is the one by Kornyshev et al[103]. These workers use a model dielectric function which smoothly varies between a free-electron model value in the bulk electrode to that of the Gouy-Chapman model in the bulk electrolyte. By choosing reasonable values for the interfacial dielectric function they are able to obtain agreement with experimental values of C_* and estimate the extent of electron spill-out to be 1-3Å, for a dilute aqueous electrolyte. A simpler version of their theory in which the elctrode has a sharp interface leads to estimates for C_* which are similar to those obtained by Rice[117] and thus far higher than experimental values.

We turn now to the potential at the point of zero charge, V^{pzc}. A considerable number of papers about V^{pzc} have been published and the latter is known[120] to depend on many factors such as solution composition, solvent and temperature. A dependence on the metal used may also be observed despite the experimental difficulties. It is this dependence that we are concerned with here.

In section 5.1 the surface potential of the free metal surface, χ^m, was related to the work function of the metal, Φ. A similar correlation is found for metal-dilute electrolyte systems between V^{pzc} and the work function. This can be seen from Figure 5.4 (a)[81] where results for aqueous electrolytes are given. This correlation is further evidence that the structure of a metal

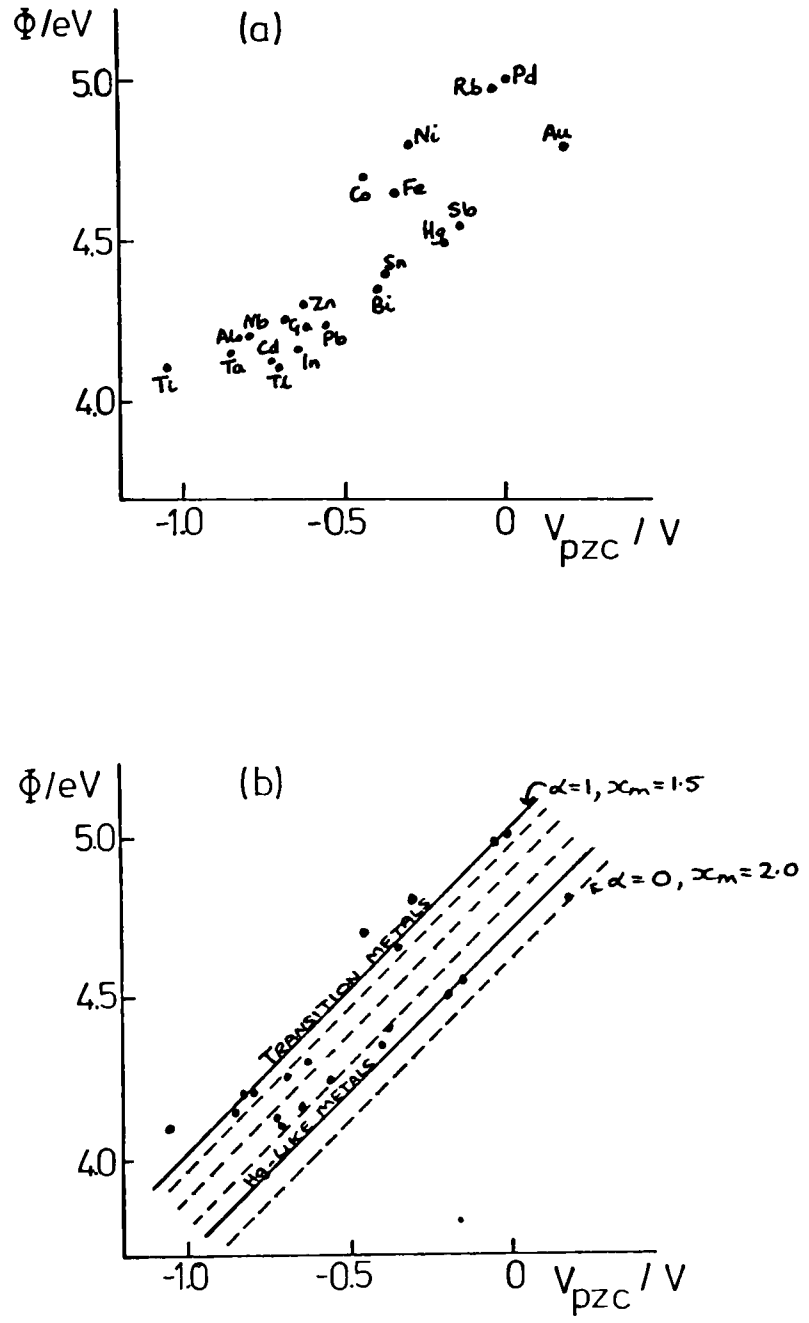


Figure 5.4 The correlation between the metal work function and the potential at the point of zero charge.

surface in contact with an electrolyte is qualitatively similar to a free metal surface.

Of course, the present problem is more complex than that of the free surface and the effect of the presence of water molecules on the potential across the interface must also be considered. In particular, the extent of alignment of the water dipoles at the surface will affect V^{pzc} . This alignment is more commonly termed 'degree of water orientation', α . α has a maximum value when the dipoles are all aligned (dipole away from the metal surface) and is at a minimum when the dipoles are randomly orientated. Using this concept, Trasatti proposed a relation[81]:

$$V^{pzc} = \Phi + a + b\alpha \qquad (5.9)$$

where a and b are adjustable parameters found to be -4.61 and -0.40 respectively. α is related to the effective electronegativity of the metal, x_m , by:

$$\alpha = \frac{2.10 - x_m}{0.6} \qquad (5.10)$$

The values of x_m , which were specifically obtained for the metal surface by Trasatti, are similar to the electronegativities of Pauling[121]. Experimental V^{pzc} values and those calculated using equations (5.9) and (5.10) for several different x_m are given in Figure 5.4 (b). Note that away from the point of zero charge α tends rapidly to unity as the water dipoles line up under the influence of the increased electrostatic forces[118]. V^{pzc} then becomes from equation (5.9) simply a function of Φ .

5.3 Phenomenological treatment of electron spill-out

In Chapter 4 we obtained results for metal-molten salt interfaces using a model in which the electrolyte is described by the mean spherical approximation and the electrode is represented as a hard wall. We obtained differential capacitance values for zero electrode charge which are of similar magnitude to the experimental ones. We concluded from this that the MSA gives the structure of the molten salt reasonably well since C^{PZC} is directly given by this structure through an integral over the wall-ion distribution functions. In Chapter 4 we also looked at the temperature dependence of C^{PZC}. Our hard wall model gives this incorrectly, the sign of the dependence being opposite to that observed. In this section we extend the theory of Chapter 4 by introducing a parameter, Δd, which we use to fit the hard wall-MSA results to the experimental results. We then show by a simple argument that Δd may be thought of as the extent of electron spill-out (or penetration) into the electrolyte.

We introduce the parameter, Δd, such that:

$$\frac{1}{C^{PZC}} = -\frac{4\pi}{\varepsilon}\Delta d + \frac{1}{C^{PZC}_{MSA}} \quad . \tag{5.11}$$

In this equation C^{PZC} is the capacitance of the new model at the PZC and C^{PZC}_{MSA} is the capacitance calculated using the hard wall-MSA model of Chapter 4. The quantity ε in equation (5.11) is the dielectric constant of the molten salt as given by the Clausius-Mossotti equation (equation (4.29). By using equation (4.26) equation (5.11) may be rewritten as:

$$C^{PZC} = \frac{\varepsilon}{4\pi} \frac{2\Gamma}{1-2\Gamma\Delta d} \qquad (5.12)$$

Values of Δd were obtained from equation (5.12) by fitting to the experimental values at different temperatures and the results of this fitting are shown in Figure 5.5.

The parameter Δd may be given a physical interpretation. Consider first the original model. In this there is a sharp interface between the metal and the electrolyte with the density of the metal electrons going to zero at the hard wall. This is shown schematically in Figure 5.6(a). So, in this model the hard wall is placed at the limit of the electron spill-out from the ion core lattice. However, the spill-out region is 'soft' so that a more appropriate position for the hard wall is at the limit of the lattice of metal ion cores. As in the original model the electrolyte ion distribution is zero inside the hard wall, but now the metal electron distribution extends beyond this hard wall and thus the interface is no longer sharp. This new model, as shown in Figure 5.6(b), is electrostatically equivalent to two capacitors in series and the overall capacitance of the interface is given by equation (5.11). Thus, Δd may be interpreted as the extent of the electron spill-out into the electrolyte. The value of ε used in equation (5.11) is quite consistent with this interpretation because of the small variation of ε between electrolyte and electrode expected for molten alkali halide systems (cf. section 4.3).

Figure 5.5 may be explained on this basis. (Note that, although lithium salts are included on this diagram, the failure of the original MSA model to account for their anomalous

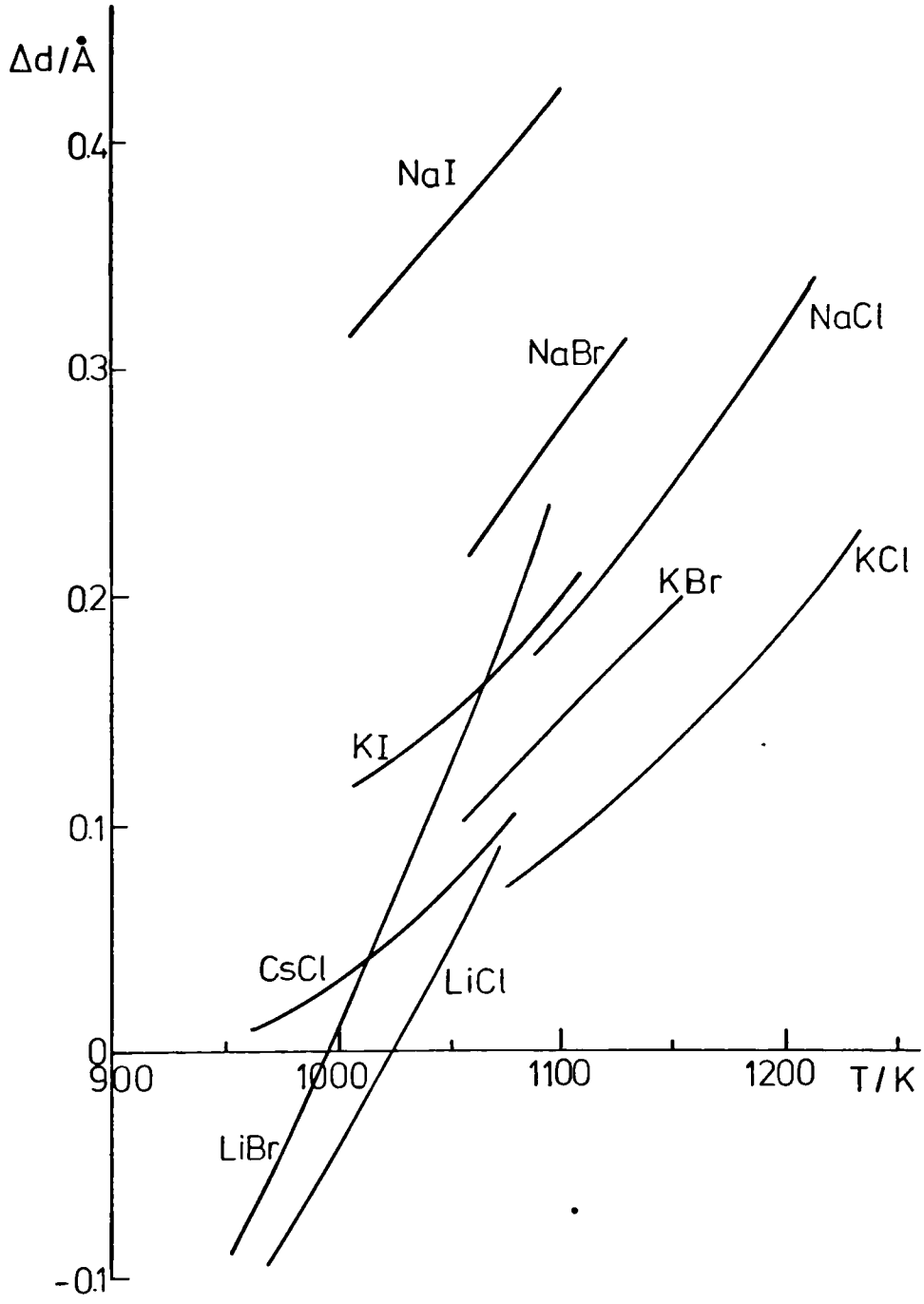


Figure 5.5 Calculated values of the fitting parameter Δd .

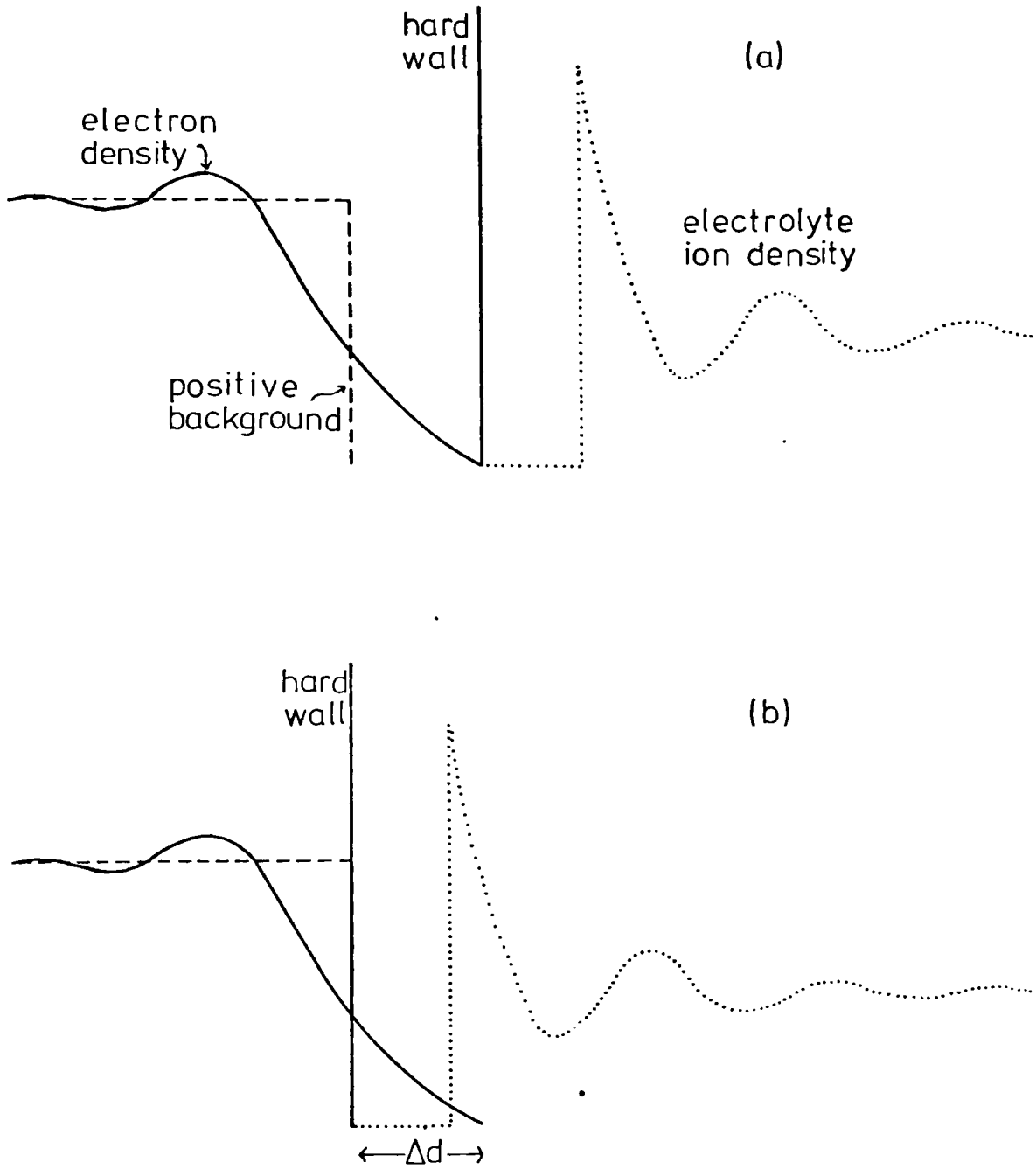


Figure 5.6 Schematic view of (a) the original model of the interface introduced in Chapter 4 and (b) the modified model.

behaviour renders the Δd values for them suspect). First, all the Δd values increase with temperature; this is presumably a result of the stabilising capacity of the electrolyte ions increasing with their kinetic energy. Similarly electrolytes with a small cation and a large anion, like NaI, will have the greatest stabilising effect on electron spill-out, and will therefore maximise Δd, whereas electrolytes with a large cation and a small anion such as CsCl will have the opposite effect. The relative magnitudes of the calculated Δd values are in agreement with this.

The inclusion of Δd as interpreted above into our original model of Chapter 4 is in keeping with the view of the interface put forward in the review earlier in this chapter, namely that the interface between the metal and the electrolyte is not sharp but diffuse. However, our numerical values are not directly comparable with those of other workers[103,112-114] because the latter have been exclusively concerned with aqueous systems. In general their predictions for the extent of spill-out are in the range 1-3 Å whereas ours are ~ 0.1-0.3 Å indicating that electrons are much more strongly stabilised by aqueous systems. One undoubted cause of this is the very high dielectric constant of water which, even in the compact layer (where the effective dielectric constant will be much lower than in the bulk), will be higher than that found in molten alkali halide systems. We must also note here the disagreement with the work of Blum[100]. He proposes a parameter formally similar to ours but with a different physical interpretation leading to a positive sign in equation (5.12). He gives no numerical results.

In summary, it may be concluded from the several strands of evidence discussed in this chapter that in all probability the metal does play a significant role in the electrical double layer and that the extent of the contribution depends on the nature of the metal. It has also been seen that to explain this role the concept of electron spill-out is of value when applied to a metal surface in contact with an electrolyte. However, the latter system is more complex than a free metal surface because electron spill-out considerations can only explain part of the electrode's contribution to the properties of the interface region.

Chapter 6 Future work

One constituent of all metal-electrolyte systems is the electrolyte. It consists of an ionic part and, possibly, a solvent. Its influence on the behaviour of the whole system depends on the chemical and physical effects of these components.

The chemical effects mentioned arise from specific short-range interactions between the electrolyte and the electrode, and between the components of the electrolyte itself. The physical effects include both electrostatic interactions and the interactions which usually fall under the heading of 'intermolecular forces'. These include the repulsive forces, which we have often modelled as a hard-wall or hard-sphere potential in this thesis, and various longer-ranged attractive forces.

Clearly then, the electrolyte alone poses formidable problems before the complications of inhomogeneity introduced by the electrode are added. Our first aim must be to minimise the number of these possible contributions which are important. As we have discussed above, careful choice of electrolyte and electrode materials can make the chemical effects negligible, to a reasonable approximation. Another obvious way of simplifying the problem is to consider solvent-free systems. Then, at least, all the complications which result from interactions with the solvent can be obviated. After all, the presence of a solvent in a metal-electrolyte system is primarily for the convenience of performing experiments and is not essential for the investigation of such systems. The use of water as a solvent is particularly hard on the theoretician as even in its pure homogeneous state its properties are very difficult to predict with any accuracy.

Tradition and this experimental convenience, however, have resulted in the large bulk of experimental and theoretical studies being made on systems with an aqueous electrolyte, as we showed in Chapter 2 and 3. The theoretical studies have several characteristics in common, notably that their agreement with each other and with computer experiments is generally better than their agreement with real experiments. It is our contention that the dominant factor which is lacking from these models is a realistic model of water. A strong piece of evidence supporting this is our work on molten salt systems. Even though we did not include any factors which were not included in the corresponding aqueous system theories, our MSA model produced considerably better agreement with experiment.

This is a promising start but more work undoubtedly needs to be done. An important step should be the setting up of a computer experiment to check the predictions of our integro-differential equation approach. Existing computer simulations of aqueous systems usually model the water as a uniform continuum simply providing a background of high dielectric constant. Therefore, it should be relatively easy to reduce the dielectric constant and increase the average ionic density in one of these simulations to provide an effective tool to study molten salt systems.

Our results for the MSA and EXP approximations show too that more closure approximations need to be evaluated for electrode-electrolyte systems (a study using the HNC approximation is already underway[108]). The difference between our results for these models show that the properties of the interface are very

sensitive to small differences in electrolyte structure. For example it does not follow that an approximation which describes the bulk structure successfully will necessarily be good for the interface: it will be remembered that EXP is generally considered to be an improvement over MSA for bulk alkali halides, whereas the relative merits of the two models for the interface are reversed.

Some properties of the interface can only be studied in the presence of a solvent - notably bulk ionic concentration dependences. In these cases the simplest examples are likely to be found in systems with non-aqueous solvents, as these generally have a much less complex structure than water. There is already evidence for this in the work of Fawcett (cf. section 3.3). His models have been relatively successful in describing non-aqueous systems, but even when specially extended they have not been as successful in describing aqueous ones.

Perhaps the next factor to consider after molten salt electrolytes is the electrode. Clearly it is characterised by physical and chemical interactions with all the constituents of the electrolyte. Providing the chemical interactions can be minimised by appropriate choice of electrode material, our work indicates that significant improvement of agreement with experiment can be expected if we go beyond modelling the electrode as a structureless charged hard wall so common in existing theories. There are a number of theories of the free metal surface which would serve as a starting point. The jellium model would seem from our work to be an appropriate one as it is still relatively simple and includes the main structural features of metals.

However, chemical interactions cannot be ignored completely. Their presence undoubtedly adds a great deal to the complexity of interfacial systems which have a considerable complexity already. A few quantitative estimates of their effect have been made by concentrating on charge-transfer interactions[54], but most of the limited number of papers in this area have been qualitative, usually involving no more than a description of the types of interactions expected[54,122]. The dearth of activity in this area owes far more to its difficulty than its lack of importance as a determinant of the behaviour of real systems.

In summary, then, a complete understanding of the electrified interface remains a remote prospect. However, progress can still be made, in particular by concentrating on systems involving molten salts or non-aqueous electrolytes when even simple models can reasonably be expected to have a chance of quantitative success. Improvement of the theoretical results for aqueous electrolytes is expected to be less easy since the main weakness of the models is the way in which the water structure is included. There is still much uncertainty about the latter for the bulk and it is not likely that this will be readily reduced. However, probably the most difficult aspect of the interface to account for theoretically is the chemical bonding between the metal, the ions and the solvent molecules. Close analysis of the experimental data should indicate the predominant interactions and so help with the understanding of the interface. In fact for all aspects of the interface problem progress should be made if emphasis is put on relating the theory to experiment.

Appendix A The Baxter technique

The factorisation method given by Baxter[99] for neutral fluids has been extended to ionic fluids by Blum and Hoye[123]. It provides a very convenient method of solution of the mean spherical approximation, an alternative being the Laplace transform method developed by Waisman and Lebowitz[124].

The first step in the Baxter method is to prove that the functions $c_{\alpha\beta}(r)$ can be written in terms of the factor correlation function matrix, $Q_{\alpha\beta}(r)$:

$$Q_{\alpha\beta}(r) = \delta_{\alpha\beta} - (n_\alpha n_\beta)^{1/2}\left[(z_\alpha a_\beta / ir)\exp(ird_{\alpha\beta}) + \int_{\lambda_{\beta\alpha}}^{d_{\alpha\beta}} dr \exp(irr) Q_{\alpha\beta}(r)\right]. \quad (A1)$$

Here, $n_{\alpha,\beta}$, $z_{\alpha,\beta}$ and $d_{\alpha,\beta}$ have the same meaning as in the main text and $\lambda_{\beta\alpha} = \frac{1}{2}(d_\beta - d_\alpha)$. The matrix elements, $Q_{\alpha\beta}$, and the coefficients a_β in equation (A1) must now be determined. This is done by considering the integral equation which defines the pair correlation function in terms of $J_{\alpha\beta}(r)$:

$$J_{\alpha\beta}(r) = 2\pi \int_r^\infty dr' r' h_{\alpha\beta}(r'). \quad (A2)$$

Combining this integral equation with the MSA condition (4.12) and (4.13) it can be proved that:

$$Q_{\alpha\beta}(r) = \tfrac{1}{3}\pi\rho\, a_\alpha (r - d_{\alpha\beta})^3 + \tfrac{1}{2} Q''_{\alpha\beta}(r - d_{\alpha\beta})^2 + Q'_{\alpha\beta}(r - d_{\alpha\beta}) - z_\alpha a_\beta \quad (A3)$$

where $\rho = \sum_\alpha z_\alpha n_\alpha$, and hence the coefficients may be obtained:

$$a_\alpha = (\alpha^2/2\Gamma) z_\alpha^* - [(\pi/2\Delta) d_\alpha^2 P]/(1 + \Gamma d_\alpha) \quad (A4)$$

$$Q'_{\alpha\beta} = (2\pi/\Delta)\, d_\alpha d_\beta \zeta_2 + (\pi^2/2\Delta^2) d_\alpha d_\beta \zeta_2 - (2\Gamma^2/\alpha^2) a_\alpha a_\beta \qquad \text{(A5)}$$

$$Q''_{\alpha\beta} = (2\pi/\Delta)\left[1 + (\pi/2\Delta) d_\beta \zeta_2 + \tfrac{1}{2} P a_\beta\right] + \pi \rho\, a_\alpha a_\beta \qquad \text{(A6)}$$

The following definitions have been used:

$$Z^*_\alpha = Z_\alpha - \tfrac{1}{6}\pi \rho\, d_\alpha^3 \qquad \text{(A7)}$$

$$P = \Omega^{-1} \sum_\alpha \left[n_\alpha Z_\alpha d_\alpha / (1+\Gamma d_\alpha)\right] \qquad \text{(A8)}$$

$$\Omega = 1 + (\pi/2\Delta) \sum_\alpha \left[n_\alpha d_\alpha^3 / (1+\Gamma d_\alpha)\right] \qquad \text{(A9)}$$

$$\Delta = 1 - \tfrac{1}{6}\pi \zeta_3 \qquad \text{(A10)}$$

$$\zeta_m = \sum_\alpha n_\alpha d_\alpha^m \qquad \text{(A11)}$$

$$\alpha^2 = 4\pi e^2/(\varepsilon kT) \qquad \text{(A12)}$$

Finally, the parameter Γ is determined by solving the equation:

$$2\Gamma = \alpha \left\{ \sum_\alpha n_\alpha \left[\frac{Z_\alpha - (\pi/2\Delta) d_\alpha^2 P}{1+\Gamma d_\alpha} \right]^2 \right\}^{1/2} \qquad \text{(A13)}$$

The quantities Z^*_α have the meaning of effective valencies, reduced from the ionic valencies Z_α by the amount of background charge contained inside the hard sphere with diameter d_α.

The results of Blum and Hoye for an ionic fluid modelled using symmetrical charged hard spheres (ie. with $d_\alpha = d_\beta = d$; $Z_\alpha = -Z_\beta = Z$) follow immediately by setting $\rho = 0$, which implies overall charge

neutrality. Then $Q_{\alpha\beta}(r)$ reduces to a second order polynomial, reduces to z_α and the last term in $Q''_{\alpha\beta}$ in equation (A6) vanishes. The expression for the parameter Γ is simplified to:

$$\Gamma d = -\frac{1}{2}\left[1-(1+2K_s d)^{\frac{1}{2}}\right]. \qquad \text{(A14)}$$

Appendix B Analytic result for the capacitance in the MSA

Consider first an isotropic, n-component electrolyte consisting of charged hard spheres of diameter d_i, density n_i and charge $z_i e$ with overall charge neutrality. In the bulk, the electric field at a distance r from a central ion of, say, species 1 is given by:

$$E(r) = E_1(r) + E_{rest}(r) \tag{B1}$$

$E_1(r)$ is the electric field due to the central ion and is given simply by $z_1 e/r^2$. $E_{rest}(r)$ is the electric field due to the remaining ions in the system and can be written in terms of the pair distribution functions of the central ion with the other ions. Using Gauss' law we obtain:

$$E_{rest}(r) = \frac{4\pi e}{r^2} \sum_k n_k z_k \int_0^r dr' r'^2 g_{1k}(r') \tag{B2}$$

The general form of the neutrality condition of Stillinger and Lovett is[125]:

$$\sum_k n_k z_k = 0 \tag{B3}$$

so we may now write $E(r)$ as:

$$E(r) = \frac{z_1 e}{r^2} + \frac{4\pi e}{r^2} \sum_k n_k z_k \int_0^r dr' r'^2 h_{1k}(r') \tag{B4}$$

where $h_{1k}(r') = g_{1k}(r') - 1$

The potential difference between the surface of the central

ion and infinity, $\Delta\psi (= \psi(d_1/2) - \psi(\infty))$, is given by:

$$\Delta\psi = z_1 e \int_{d_1/2}^{\infty} \frac{dr}{r^2} + 4\pi e \sum_k n_k z_k \int_{d_1/2}^{\infty} \frac{dr}{r^2} \int_{d_1/2}^{r} dr' r'^2 h_{1k}(r') \qquad \text{(B5)}$$

the solution of which in the MSA is:

$$\Delta\psi = \frac{2 z_1 e}{d_1} + 2e \sum_k{}' n_k z_k J_{1k} \qquad \text{(B6)}$$

where:

$$\sum_k n_k z_k J_{1k} = N_1 - \frac{\pi}{6} \sum_k n_k d_k^3 N_k - \frac{\pi}{4} \phi_2 \qquad \text{(B7)}$$

with $\phi_2 = \sum_k n_k z_k d_k^2$ and $N_i = \frac{1}{(1+\Gamma d_i)} \left\{ \Gamma z_i + \frac{\pi d_i}{2\Delta} P \right\}$.
Δ , P and Γ are as defined in Appendix A.

As in section 4.2 we may model an (n-1)-component electrolyte in contact with a hard wall by letting one type of particle, in this case species 1, become very large in size but low in concentration[30] (cf. equations (4.4) and (4.5)). In the limit species 1 becomes equivalent to a planar hard wall. Thus, in equation (B7) the sum $\sum_{k=1}{}' n_k d_k^3 N_k$ becomes instead $\sum_{k=2} n_k d_k^3 N_k$ and the functions ϕ_2 , Δ , P and Γ take forms appropriate to an (n-1)-component system. The potential difference is then given by:

$$\Delta\psi = \frac{2 z_1 e}{d_1} - \frac{2 z_1 e \Gamma}{1+\Gamma d_1} + \text{terms independent of } z_1 e \qquad \text{(B8)}$$

The differential capacitance is readily obtained using equation (1.8)

$$C = \frac{1}{\pi d_1^2} \frac{\partial(z_1 e)}{\partial(\Delta\psi)} \qquad \text{(B9)}$$

which gives:

$$C = \frac{1 + \Gamma d_1}{2\pi d_1} \tag{B10}$$

In the limit $d_1 \to \infty$ equation (B10) reduces to:

$$C = \frac{1}{4\pi} \cdot 2\Gamma \tag{B11}$$

which is in agreement with Blum's result for a restricted primitive electrolyte[100]. Here, we have shown that equation (B11) holds for a more general system, namely a multicomponent liquid containing hard sphere ions of different sizes and carrying unequal charges. In addition, it is clear that the capacitance is independent of the charge on the wall.

Appendix C Separation of the MSA capacitance into compact and diffuse layer contributions

As discussed in Chapters 2 and 3, it is common to write the capacitance of the interface as (cf. equation (2.18)):

$$\frac{1}{C} = \frac{1}{C_c} + \frac{1}{C_d} \tag{C1}$$

Consider the case of charged hard spheres of equal diameters, $d_+ = d_- = d$. The distance of closest approach is then $d/2$ and the capacitance of the charge-free compact layer is given by:

$$C_c = \frac{\varepsilon}{4\pi} \cdot \frac{2}{d} \tag{C2}$$

Thus, from the above two equations and equation (4.26) the diffuse layer capacitance is given by:

$$C_d = \frac{\varepsilon}{4\pi} \frac{K_D}{1 - \Gamma^2 d^2} \tag{C3}$$

As a function of temperature C_d diverges at $K_D d = 4$ and is negative for stronger couplings, particularly in the molten salt range. This behaviour of equation (C3) reflects the marked charge ordering in the molten salt and the existence of negative and positive values of C_d separated by a singularity cautions against the use of equation (C1), at least in the MSA.

Appendix D The exponential approximation applied to a two-component system near a hard wall

The exponential approximation was first suggested by Andersen and Chandler[36]. It has no physical basis but its use was justified by these authors since it significantly increases the rate of convergence of the numerical solution of pair distribution functions, $g_{\alpha\beta}(r)$. The approximation itself may be simply written for bulk electrolytes modelled as charged hard spheres:

$$g^{EXP}_{\alpha\beta}(r) = g^{\circ}_{\alpha\beta}(r) \exp\{A_{\alpha\beta}(r)\} \qquad (D1)$$

where $g^{\circ}_{\alpha\beta}(r)$ are the correlation functions for uncharged hard spheres; they are equal to those obtained from the Percus-Yevick equation (equation (2.28)) for hard spheres. $A_{\alpha\beta}(r)$ are so-called renormalised potentials introduced by Morita and Hiroike[127] because their inclusion simplifies diagram summation in perturbation theory. We are not concerned with the details here, but for the MSA $A_{\alpha\beta}(r)$ is given by:

$$A_{\alpha\beta}(r) = g^{MSA}_{\alpha\beta}(r) - g^{\circ}_{\alpha\beta}(r) \equiv \Delta g_{\alpha\beta}(r) \qquad (D2)$$

Thus, the correlation functions to be obtained for the interface system are:

$$g^{EXP}_{ij}(x) = g^{PZC}_{ij}(z) \exp\{\Delta g_{ij}(x)\} \qquad (D3)$$

The $g^{PZC}_{ij}(r)$ have already been obtained from the MSA calculations,

but $\Delta g_{wj}(r)$ must now be calculated.

We start from equation (4.20) and combining this with equation (4.21) obtain:

$$\Delta g_{wj}(x) - \sum_{l=1}^{2} n_l \int_{\lambda jl}^{x-d_l/2} dr\, \Delta g_{wl}(x-r) Q_{lj}(r) = -F_j(x) \qquad \text{(D4)}$$

Blum[99] has shown that in the MSA $F_j(x)$ is a constant:

$$F_j = -\frac{4\pi\beta e^2}{\varepsilon} \sigma_m M_j \qquad \text{(D5)}$$

where Blum's expression for M_j for equal diameters may be extended to the more general case giving:

$$M_j = \frac{(-1)^j g_{wi}(d_i/2)}{n[a_1 g_{w1}^{pzc}(d_2/2) - a_2 g_{w2}^{pzc}(d_1/2)]} \qquad i \neq j \qquad \text{(D6)}$$

a_1 and a_2 are the coefficients defined in Appendix A and the ionic valencies have been assumed to be +1 and -1. Equation (D4) may now be solved numerically to give $\Delta g_{wj}(x)$.

The capacitance at the point of zero charge can now be obtained. Combining equations (D4) and (D5) shows that $\Delta g_{wj}(x)$ depends linearly on σ_m, the charge on the wall. Writing this explicitly by defining a new quantity $\Delta g'_{wj}(x)$:

$$\Delta g_{wj}(x) = \sigma_m \Delta g'_{wj}(x) \qquad \text{(D7)}$$

Equation (D3) may then be written:

$$g_{wj}^{exp}(x) = g_{wj}^{pzc}(x) \exp\{\sigma_m \Delta g'_{wj}(x)\} \qquad \text{(D8)}$$

and the potential drop across the interface obtained using Gauss' law:

$$\Delta\psi = \frac{4\pi\bar{e}n}{\varepsilon}\int_0^\infty dx\, x\left[g_{w1}^{pzc}(x)\exp\{\sigma_m \Delta g'_{w1}(x)\} - g_{w2}^{pzc}(x)\exp\{\sigma_m \Delta g'_{w2}(x)\}\right] \quad \text{(D9)}$$

Using equation (1.8) the capacitance at the point of zero charge is given by:

$$\left(C_{EXP}^{pzc}\right)^{-1} = \left.\frac{\partial \Delta\psi}{\partial \sigma_m}\right|_{\sigma_m=0} = \frac{4\pi\bar{e}n}{\varepsilon}\int_0^\infty dx\, x\left[g_{w1}^{pzc}(x)\Delta g'_{w1}(x) - g_{w2}^{pzc}(x)\Delta g'_{w2}(x)\right] \quad \text{(D10)}$$

Equation (D10) must be solved numerically.

Unlike the MSA, in the exponential approximation the differential capacitance of the interface does depend on the charge on the wall. However, away from the PZC this latter approximation does not neccesarily satisfy the neutrality condition. Thus, before the capacitance at other points is calculated this condition must be included in equation (D3). This is not particularly easy to do but one suggestion has been given by Henderson and Blum[37]. Here, we have not calculated values of the capacitance other than at the PZC because of the rather poor results we obtained for C^{pzc} using the EXP approximation.

In Figure D1 the calculated inverse capacitances, using parameters corresponding to molten alkali halides, are plotted against T/T_m. The magnitude of the predicted capacitance is considerably smaller than either the experimental or the MSA values (see Figures 4.1 and 4.3). The EXP approximation does, however, predict the correct sign of the temperature dependence of C^{pzc} although quantitatively it is a stronger dependence

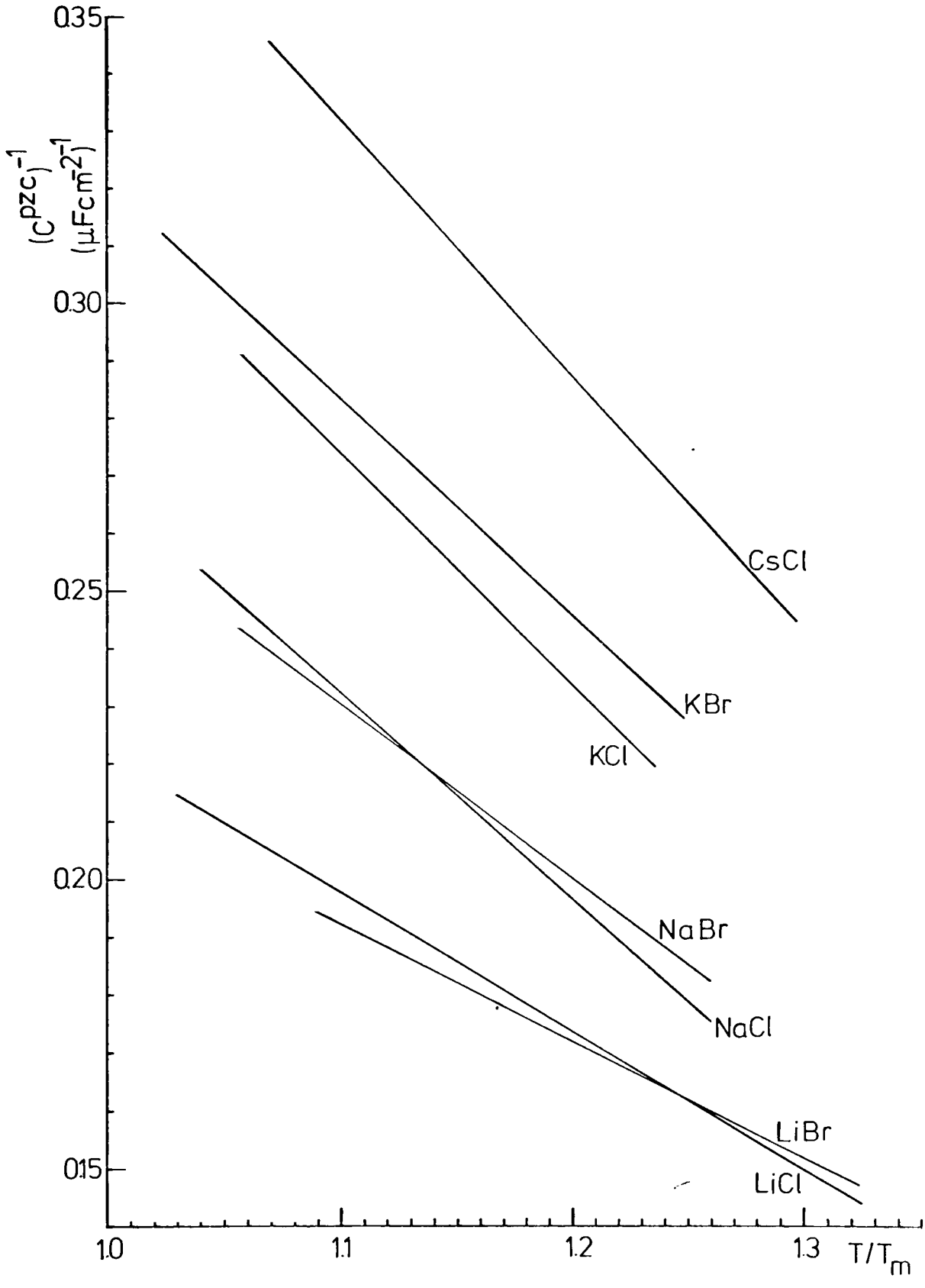


Figure D1 Inverse capacitance values calculated in the EXP approximation as a function of T/T_m .

than the one observed. These marked differences in the predictions of the two approximations are almost completely absent in their predictions for bulk molten salts[93].

Examination of the integrands in equation (D10) and the corresponding MSA expression reveals that they are of a very similar form but differ considerably in magnitude. Moreover, the bulk of the capacitance arises from the short-range behaviour of these integrands between the hard-wall contact value and the first node. Thus it is because the contact values of the wall-ion distribution function of the EXP approximation are much larger than those of the MSA that the former approximation gives rise to smaller capacitance values.

References

1. J. O'M. Bockris & A. K. N. Reddy, 'Modern Electrochemistry' (Plenum Press 1970).

2. See, for example, Comp. Treat. Electrochem 3(1981), 'Electrochemical Energy Conversion and Storage'.

3. W. R. Grove, Phil. Mag. 14(1839)127.

4. Comp. Treat. Electrochem. 4(1981), 'Electrochemical Materials Science'.

5. D. C. Grahame & R. W. Whitney, J. Am. Chem. Soc. 64(1942)1548.

6. D. C. Grahame, Chem. Rev. 41(1947)441.

7. R. Parsons, Comp. Treat. Electrochem. 1(1980)1.

8. G. Lippmann, Ann. Chim. Phys. 5(1875)494.

9. R. P. Feynman, R. B. Leighton & M. Sands,'Lectures on Physics' (Addison-Wesley 1963).

10. J. C. Rasaiah & H. L. Friedman, J. Chem. Phys. 48(1968)2742.

11. G. Gouy, J. Phys. 9(1910)457; Ann. Phys. 7(1917)129.

12. D. L. Chapman, Phil. Mag. 25(1913)475.

13. L. S. Ornstein & F. Zernike, Proc. Akad. Sci. (Amsterdam) 17 (1914)793, reproduced in H.Frisch & J. L. Lebowitz, 'The Equilibrium Theory of Classical Fluids' (Benjamin 1964).

14. S. H. Liu, Surf. Sci. 101(1980)49.

15. J. R. Macdonald, Surf. Sci. 116(1982)135.

16. D. A. McQuarrie, 'Statistical Mechanics' (Harper & Row 1976).

17. P. Debye & E. Huckel, Physik. Z. 24(1923)185,305.

18. R. Reeves, Comp. Treat. Electrochem. 1(1980)83.

19. O. Stern, Z. Elektrochem. 30(1924)508.

20. J. P. Valleau & G. M. Torrie, J. Chem. Phys. 76(1982)4623.

21. L. B. Bhuiyan, L. Blum & D. Henderson, J. Chem. Phys. 78(1983) 442.

22. D. C. Grahame, J. Chem. Phys. 21(1953)1054.

23. S. Levine & C. W. Outhwaite, J. Chem. Soc., Faraday Trans. II 74(1978)1670.

24. C. W. Outhwaite, L. B. Bhuiyan & S. Levine, J. Chem. Soc., Faraday Trans. II 76(1980)1388.

25. C. W. Outhwaite & L. B. Bhuiyan, J. Chem. Soc., Faraday Trans. II 78(1982)775.

26. J. G. Kirkwood, J. Chem. Phys. 2(1934)767.

27. J. P. Hansen & I. R. MacDonald, 'Theory of Simple Liquids' (Academic 1976).

28. D. Henderson, F. F. Abraham & J. A. Barker, Mol. Phys. 31 (1976)1291.

29. M. Born & M. S. Green, 'A General Kinetic Theory of Liquids' (C.U.P. 1949).

30. D. Henderson, L. Blum & L. B. Bhuiyan, Mol. Phys. 43(1981)1185.

31. J. G. Kirkwood, J. Chem. Phys. 3(1935)300.

32. J. K. Percus & G. J. Yevick, Phys. Rev. 110(1958)1.

33. J. M. J. Van Leeuwen, J. Groeneveld & J. de Boer, Physica 25(1959)792.

34. D. Henderson & L. Blum, J. Electroanal. Chem. 93(1978)151.

35. J. L. Lebowitz & J. K. Percus, Phys. Rev. 144(1966)251.

36. H. C. Andersen & D. Chandler, J. Chem. Phys. 57(1972)1918.

37. D. Henderson & L. Blum, J. Chem. Phys. 69(1978)5441.

38. D. Henderson, L. Blum & J. L. Lebowitz, J. Electroanal. Chem. 102(1979)315.

39. T. L. Croxton & D. A. McQuarrie, Mol. Phys. 42(1981)141.

40. D. N. Card & J. P. Valleau, J. Chem. Phys. 52(1970)6232.

41. J. C. Rasaiah, D. N. Card & J. P. Valleau, J. Chem. Phys. 56(1972)248.

42. J. P. Valleau & L. K. Cohen, J. Chem. Phys. 72(1980)5935.

43. J. P. Valleau, L. K. Cohen & D. N. Card, J. Chem. Phys. 72(1980)5942.

44. W. van Megen & I. K. Snook, Mol. Phys. 39(1980)1043.

45. W. van Megen & I. K. Snook, J. Chem. Phys. 73(1980)4656.

46. I. K. Snook & W. van Megen, J. Chem. Phys. 75(1981)4104.

47. G. M. Torrie & J. P. Valleau, Chem. Phys. Lett. 65(1979)343.

48. G. M. Torrie & J. P. Valleau, J. Chem. Phys. 73(1980)5807.

49. M. Lozada-Cassou, R. Saavedra-Barrera & D. Henderson, J. Chem. Phys. 77(1982)5150.

50. G. M. Torrie, J. P. Valleau & G. N. Patey, J. Chem. Phys. 76(1982)4615.

51. L. B. Bhuiyan, C. W. Outhwaite & S. Levine,Mol. Phys. 42 (1981)1271.

52. M. Gouy, Ann. Chim. Phys. (7)29(1903)145; (8)8(1906)291; (8)9(1906)75.

53. A. Frumkin, Z. Physik. Chem. 103(1923)43,55; 109(1924)34.

54. M. A. Habib & J. O'M. Bockris, Comp. Treat. Electrochem. 1(1980)135.

55. D. C. Grahame, E. M. Coffin, J. I. Cummings & M. A. Poth, J. Am. Chem. Soc. 74(1952)1207.

56. Most of this work is published in Soviet Electrochemistry, recent papers are V. A. Bulavka, N. B. Grigor'ev & Yu. M. Loshkarev, 14(1978)899,1204; I. A. Bagotskaya & L. M. Dubova, 13(1977)49.

57. R. Parsons, Electrochim. Acta 21(1976)681.

58. D. C. Grahame, J. Am. Chem. Soc. 76(1954)4819.

59. D. C. Grahame, Z. Elektrochem. 59(1955)740.

60. D. C. Grahame, Report No. 14 to the Office of Naval Reasearch February 18, 1954.

61. P. Holmqvist, J. Electroanal. Chem. 68(1976)31.

62. R. Parsons & S. Trasatti, Trans. Faraday Soc. 65(1969)3314.

63. J. Lawrence, R. Parsons & R. Payne, J. Electroanal. Chem. 16(1968)193.

64. D. C. Grahame, J. Am. Chem. Soc. 80(1958)4201.

65. R. Grand, C. R. C. Acad. Sci. Påris C275(1972)981.

66. J. O'M. Bockris, K. Muller, H. Wroblowa & Z. Kovac, J. Electroanal. Chem. 10(1965)416.

67. S. Minc & M. Jurkiewicz-Herbich, J. Electroanal. Chem. 34 (1972)351.

68. J. R. Macdonald, J. Chem. Phys. 22(1954)763.

69. A. de Battisti & S. Trasatti, J. Electroanal. Chem. 59 (1975)137.

70. R. Payne, J. Electroanal. Chem. 60(1975)183.

71. A. de Battisti, B. A. Abd-El-Nabey & S. Trasatti, Trans. Faraday Soc. I 72(1976)2076.

72. R. Payne, J. Electrochem. Soc. 113(1966)999.

73. B. G. Dekker, M. Sluyters-Rehbach & J. H. Sluyters, J. Electroanal. Chem. 21(1969)137.

74. I. R. Miller & H. Great, Electrochim. Acta 15(1970)1143.

75. S. Minc & M. Jurkiewicz-Herbich, J. Electroanal. Chem. 40(1972)229.

76. D. C. Grahame, J. Am. Chem. Soc. 79(1957)2093.

77. H. Buhl, Electrochim. Acta 16(1971)1495.

78. H. Buhl, Coll. Czech. Chem. Comm. 36(1971)781.

79. D. C. Grahame, J. Chem. Phys. 23(1955)1725.

80. S. Trasatti, J. Electroanal. Chem. 91(1978)293.

81. S. Trasatti, J. Electroanal. Chem. 33(1971)351.

82. S. Trasatti, Adv. Electrochem. Electrochem. Eng. 10(1977)213.

83. R. J. Watts-Tobin, Phil. Mag. 6(1961)133.

84. W. R. Fawcett, J. Phys. Chem. 82(1978)1385.

85. D. Eisenberg & W. Kauzmann, 'The Structure & Properties of Water' (OUP 1969).

86. W. R. Fawcett, S. Levine, R. M. de Nobriga & A. C. McDonald, J. Electroanal. Chem. 111(1980)163.

87. Z. Borkowska, R. M. de Nobriga & W. R. Fawcett, J. Electroanal. Chem. 124(1981)263.

88. S. L. Carnie & D. Y. C. Chan, J. Chem. Phys. 73(1980)2949.
J. Chem. Phys. 74(1981)1472.

89. P. Delahay, 'Double Layer & Electrode Kinetics', (Interscience 1965).

90. I. Langmuir, J. Am. Chem. Soc. 40(1918)1361.

91. J. O'M. Bockris, M. A. V. Devanthan & K. Muller, Proc. Roy. Soc. Lond. A274(1963)55.

92. A. D. Graves & D. Inman, J. Electroanal. Chem. 25(1970)357.

93. M. Parrinello & M. P. Tosi, Riv. N. Cimento 2(1979)1.

94. N. H. March & M. P. Tosi, 'Charged Liquids' (Academic, in press)

95. J. D. Eshelby, C. W. A. Newey, P. L. Pratt & A. B. Liddiard, Phil. Mag. 3(1958)75.

96. J. R. Hardy & A. M. Karo, 'The Lattice Dynamics & Statics of Alkali Halide Crystals' (Plenum 1969).

97. M. C. Abramo, C. Caccamo, G. Pizzimenti, M. Parinello & M. P. Tosi, J. Chem. Phys. 68(1978)2889.

98. L. Blum & G. Stell, J. Stat. Phys. 15(1976)439.

99. R. J. Baxter, J. Chem. Phys. 52(1970)4559.

100. L. Blum, J. Phys. Chem. 81(1977)136.

101. G. J. Janz, 'Molten Salt Handbook' (Academic 1967).

102. M. Born & K. Huang, 'Dynamical Theory of Crystal Lattices' (OUP 1954).

103. A. A. Kornyshev, W. Schmickler & M. A. Vorotyntsev, Phys. Rev. B25(1982)5244.

104. G. W. Ford & W. H. Weber, Surf. Sci. 110(1981)L587.

105. E. A. Ukshe, N. G. Bukun, D. I. Leikis & A. N. Frumkin, Electrochim. Acta 9(1964)431.

106. E. A. Ukshe & I. V. Tomskikh, Doklady Phys. Chem. 150(1963)416.

107. M. V. Smirnov, V. P. Stepanov & A. F. Sharov, Doklady Phys. Chem. 197(1971)288.

108. Numerical results are expected shortly from M. P. Tosi et al., ICTP, Trieste.

109. F. Garcia-Moliner & F. Flores, 'Introduction to the Theory of Solid Surfaces' (CUP 1979).

110. E. Lange, Z. Elektrochem. 55(1951)76.

111. R. Parsons, Mod. Aspects Electrochem. 1(1954)103.

112. N. D. Lang & W. Kohn, Phys. Rev. B1(1970)4555.

113. N. D. Lang & W. Kohn, Phys. Rev. B3(1971)1215.

114. S. Trasatti, Comp. Treat. Electrochem. 1(1980)45.

115. J. C. Riviere, in Solid State Surface Science, ed. M. Green, Vol 2 (Marcel Dekker 1969).

116. S. Trasatti, J. Chim. Phys. 72(1975)561.

117. O. K. Rice, Phys. Rev. 31(1958)1051.

118. A. N. Frumkin, B. B. Damaskin, N. Grigoryev & I. Bagotskaya, Electrochim. Acta 19(1974)69.

119. N. W. Ashcroft & N. D. Mermin, 'Solid State Physics' (Holt, Rinehart & Winston 1976).

120. A. N. Frumkin, O. A. Petrii & B. B. Damaskin, Comp. Treat. Electrochem. 1(1980)221.

121. L. Pauling, 'The Nature of the Chemical Bond' (Univ. Press Ithaca NY 1960).

122. S. K. Rangarajan, Electrochem., Spec. Per. Rep., Chem. Soc., 7(1980)203.

123. L. Blum & J. S. Høye, J. Phys. Chem. 81(1977)1311.

124. E. Waisman & J. L. Lebowitz, J. Chem. Phys. 56(1972)3086,3093.

125. F. H. Stillinger & R. Lovett, J. Chem. Phys. 49(1968)1991.

126. L. Blum, Mol. Phys. 30(1975)1529.

127. T. Morita & K. Hiroike, Prog. Theor. Phys. 25(1961)537.